Chapter 6

RESULT AND DISCUSSION

6.1 Introduction

After extensive data collection throughout the year, it has been found that the condenser surface's tilt angle from horizontally plays a crucial role in improving the efficiency of solar still. Also, different solar still designs with advanced materials improve the yield. The observations have been taken throughout the daylight period from 9:00 to 17:00 and the nocturnal period from 17:00 to 24:00. One-year data has been collected and analyzed to obtain optimum design and material for improved yield.

6.2 Effect of tilt angle on SS

Generally, the optimum tilt angle was set according to the latitude angle of the location (latitude angle), but it gets influenced by the seasons and location. It may be less than, equal to, or greater than the latitude angle of location, as summarized. The first part of the investigation discusses the effect of tilt angle on yield and efficiency. Daylight and nocturnal productivity variation with time have been explored in the early winter season of the composite climate of India. In low and moderate solar insolation conditions, tilt angles play a critical role. Additionally, it highlights that nocturnal productivity can be significantly improved by covering the condenser surface by insulating material at night time.

6.2.1 Hourly variation of climate condition

Model-1 and Model-2 both are SBSS faced toward the south direction while Model-3 SBDS were faced toward the east-west direction. Multiple experiments were conducted on various

days. Among them, three days' outcomes are presented here. Three days are namely, Day-1 (Oct 28, 2019), Day-2 (Oct 29, 2019), and Day-3 (Nov 5, 2019).

Figure 6.1, 6.2, and 6.3 represents the variation of solar insolation (I_s) and ambient temperature (T_a) with time. Observations showed that maximum insolation received by Model-2 and minimum by Model-3 in the same climatic condition due to different tilt angles that provides a marginally large area for solar flux entrance for Model-1 relative to Model-3. During these three days, Model-1 and Model-2 have registered an average solar insolation of 518, 416, 512 W/m^2 and 566, 456, 564 W/m^2, while Model-3 has registered an average solar insolation of around 436, 372, 423 W/m^2. The maximum solar insolation was recorded from 11:00 to 12:00 o'clock. After this period, solar flux keeps mitigating till the end of daylight. Figure 6.2, Day-2 showed an abrupt fall in solar flux after peak insolation value, and it occurs near the observation point, which can be possible due to the presence of cloudy weather. The variation in tilt angle influences the interception of solar insolation significantly. In the winter, the angle of the incident of solar insolation gets changed compared to the summer season, which is why maximum radiation is trapped for Model-2 instead of Model-1, which has a tilt angle close to the latitude angle. Model-1 showed mediocre performance in solar power interception, and its low tilt angle causes a thicker film of condensate that further hampers the condensation rate of vapor. Model-3 showed the least trapping of solar insolation due to its orientation and slope. The east-west orientation is suited when the zenith angle is minimum. The maximum impressment of solar insolation leads to the high-temperature gradient inside the basin that eventually augment the productivity and efficiency of the still.

It also indicates the variation of ambient temperature (T_a) on the secondary y-axis that has a

common trend for all three models, and it is trivial that T_a does not depend upon the model geometry. In contrast, an almost invariable trend is recorded in all three days. The maximum temperature is obtained around 13:30. The time lags between maximum insolation and maximum ambient temperature indicate the high heat capacity of air and cloudy weather.

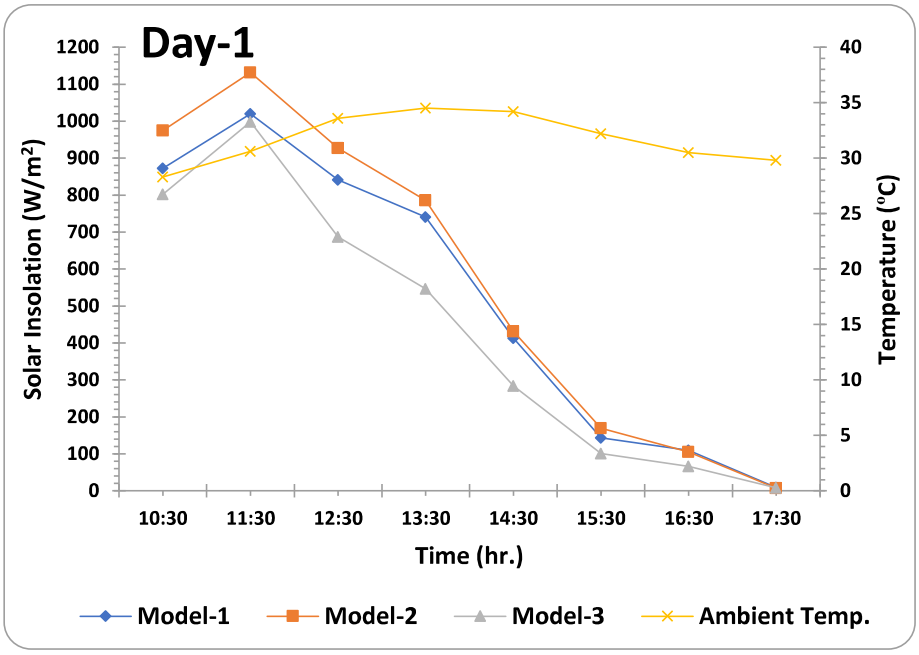

Figure 6. 1Hourly variation of solar insolation and Ambient temperature with three models on Day-1

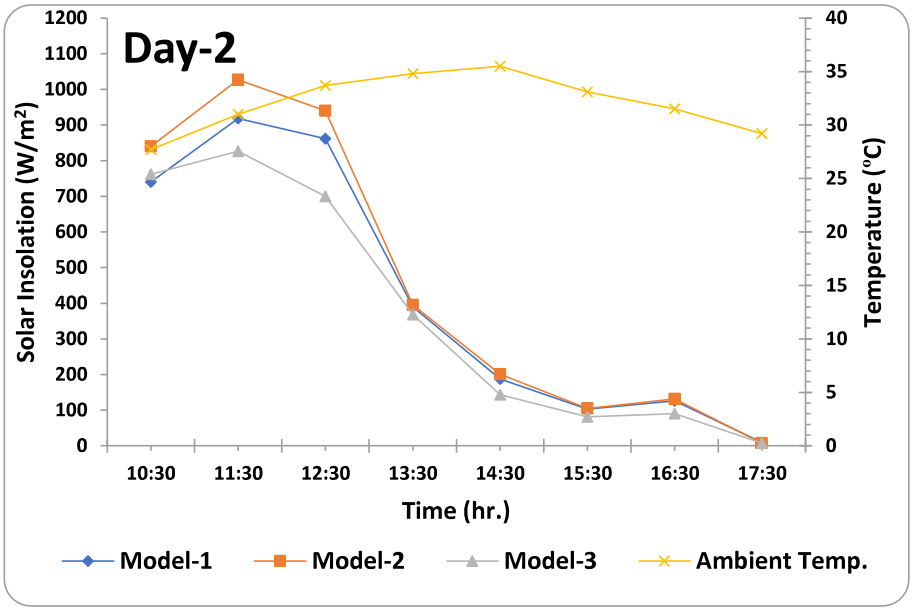

Figure 6. 2 Hourly variation of solar insolation and Ambient temperature with three models on Day-2

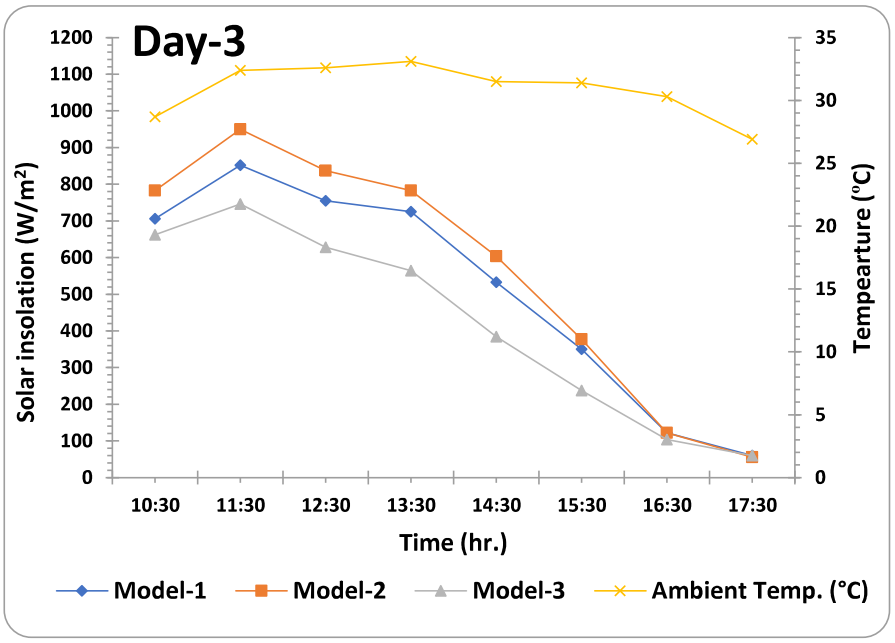

Figure 6. 3 Hourly variation of solar insolation and Ambient temperature with three models on Day-3.

6.2.2 Variation of SS inside condition and Yield

Figure 6.4 shows the hourly variation of basin water temperature (T_w) and inner glass temperature (T_{ig}). It can be observed that Model-2 can achieve a maximum basin water temperature of 57º C at 13:30 hr. relative to others during the experiment. Also, the inner basin water temperature increased for model-1 and Model-2. In contrast, model-3 shows reverse behavior, which can be explained by the low rate of condensation at the surface that causes low latent heat liberation compared to others. It was noticed that the average temperature difference between basin water and inner glass surface maximum for Model-3 was around 18.1ºC as compared to model-1 and model-2, which have 5.3ºC and 11.3ºC, respectively. Although Model-3 depicts a good condition of desalination however, due to its low tilt angle (15º), condensed droplets are not able to glide down quickly into the collector, causing a thick of condensate formed on the glass cover that results in the fall of condensate back into the basin.

Figure 6.5 shows the hourly yield variation and cumulative yield of three models. At 13:30 hr., model-1 produces a maximum of 230 mL while model-2 yields 170 mL. It was found that model-3 basin water temperature was higher than model-1. However, their corresponding yields have no significant difference after 16:30 hr., which happens due to the low tilt angle (15º) of the glass cover of model-3, which creates an unfavorable slope for condensed droplets to glide down. However, Model-1 has a 25º tilt angle higher than Model-3, producing nearly the same output instead of low basin water temperature. Its higher slope makes condensate more favorable for gliding down in the trough.

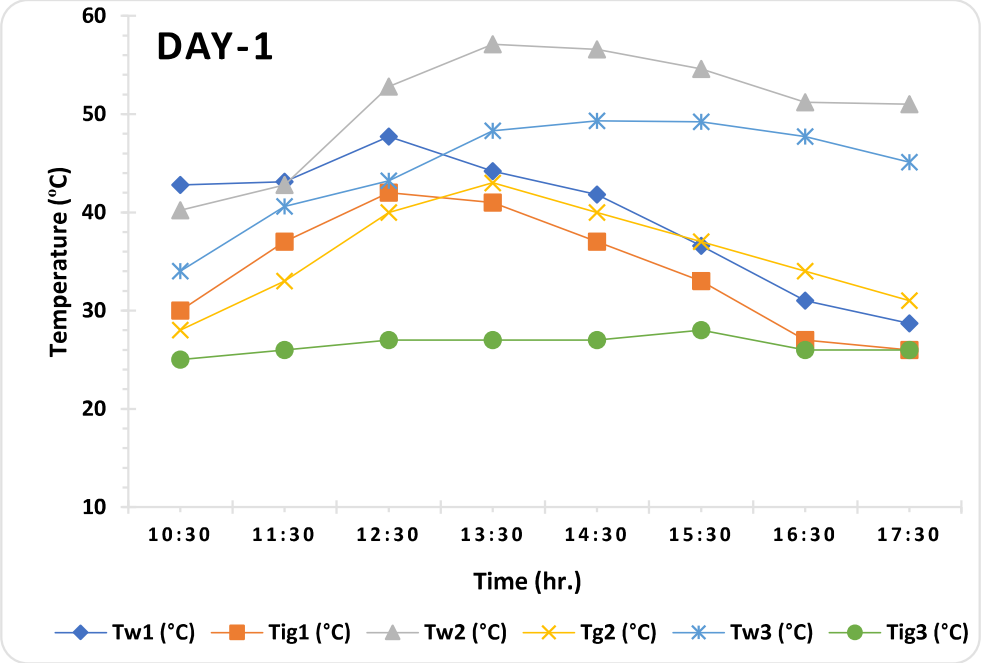

Figure 6. 4 Hourly variation of basin water and inner glass surface temperature on Day-1

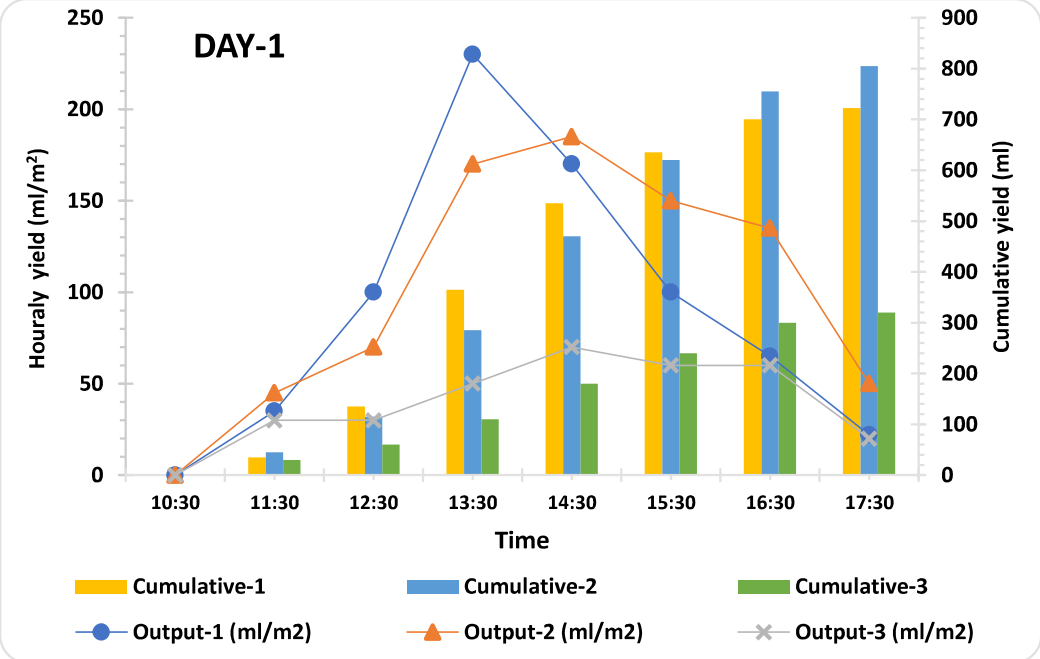

Figure 6. 5 Hourly variation of productivity during daylight time on Day-1

Figure 6.6 shows the Day-2 variation of basin water temperature and inner glass surface. That shows model-2 has a higher average basin water temperature than model-3 and model-1. The maximum basin water temperature attained by model-2 and model-3 was 56.1ºC and 48ºC at 14:30 hr., while model-1 achieved the highest temperature, 46 ºC at 11:30 hr. This variation is due to different tilt angles of condenser surfaces. Whereas, Figure 6.7 shows hourly yield variation with respect to time and cumulative yield. On day-2, nearly the same results were obtained except for variation in hourly yield. At 15:30 hr., model-2 produces a maximum yield of 180 mL while model-1 produces 130 mL

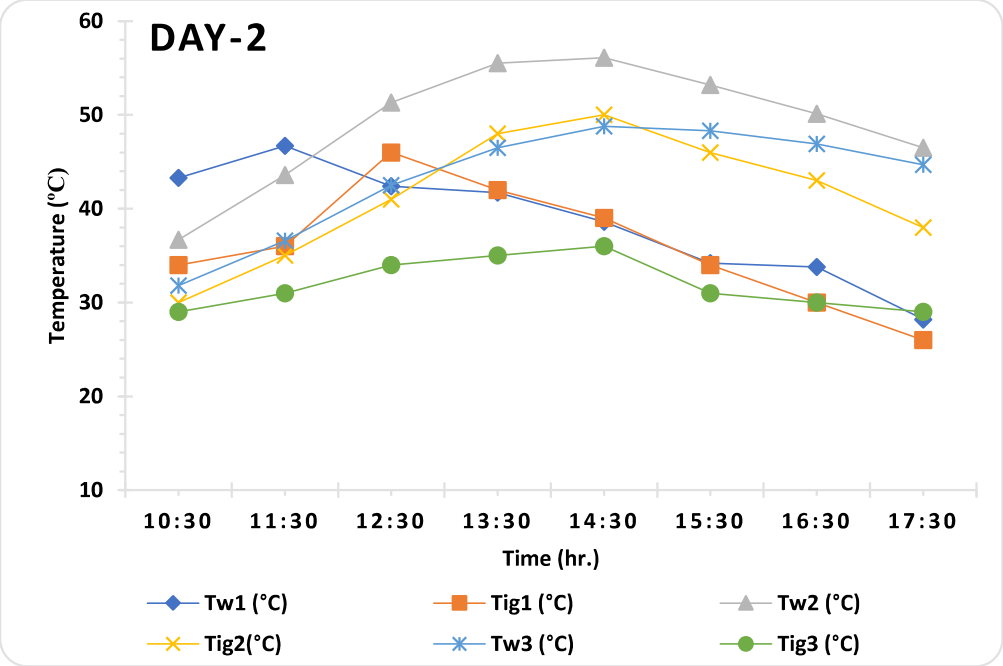

Figure 6. 6 Hourly variation of basin water and inner glass surface temperature on Day-2

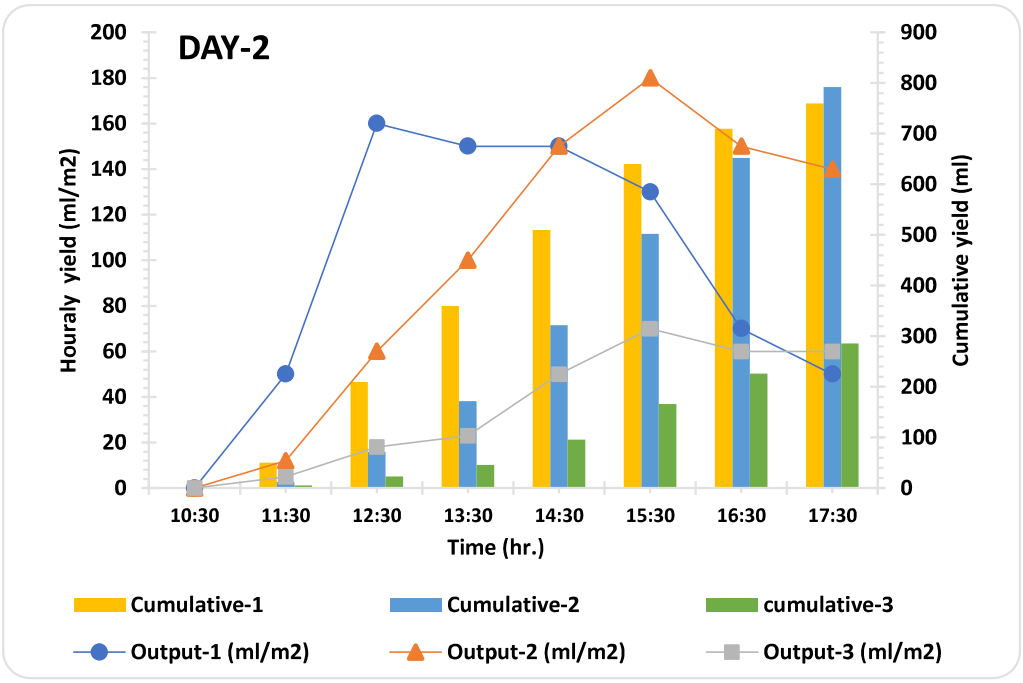

Figure 6. 7 Hourly variation of productivity during daylight time on Day-2

The Figure 6.8 shows hourly variation of basin water and inner glass surface temperature on day-3. The maximum basin water temperature was achieved by model-1 earlier than model-2 and model-3. On day-3, model-1 achieved maximum 47ºC around 13:00 hrs. whereas, model-2 and model-3 achieved maximum temperature of 55ºC and 48ºC at 14:30 hrs. that shows model-1 achieved its maximum temperature earlier than others. The temperature difference was always a crucial parameter for the process of solar desalination. Figure 6.9 shows the hourly yield and cumulative yield that shows rate of increase of yield was maximum for the mode-2 with maximum output of 190 mL/m^2 at 13:30 hr. The yield was obtained nearly one hour after the maximum basin water temperature condition as on day-3. That can be taken as response time of SS. The model-1 and model-2 has response time of one hour since every time maximum yield obtained after one hour of highest basin water temperature. Whereas, model-3 has larger response time noticed from the experimental

observation.

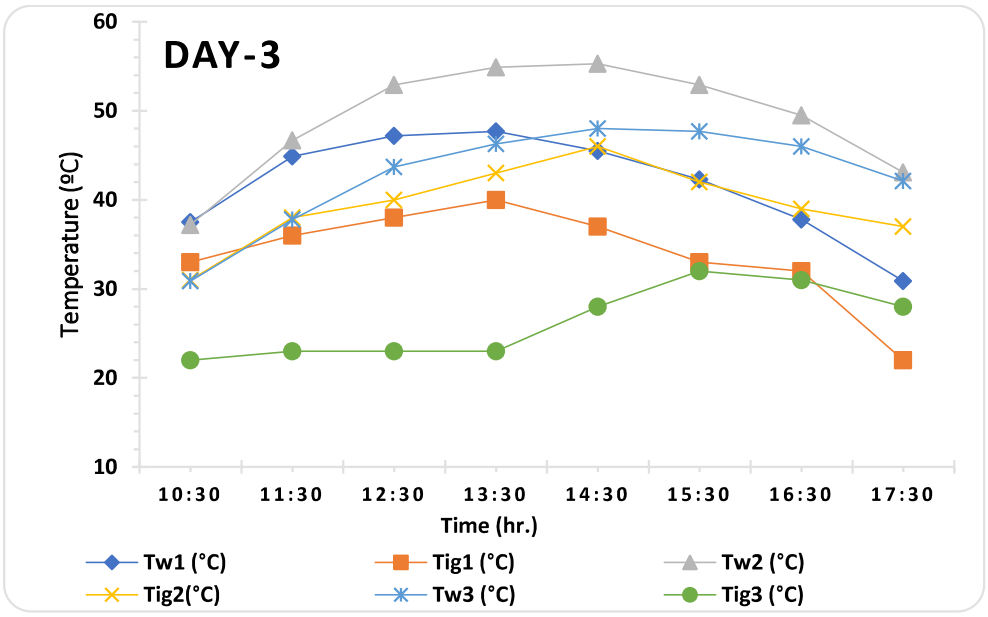

Figure 6. 8 Hourly variation of basin water and inner glass surface temperature on Day-3

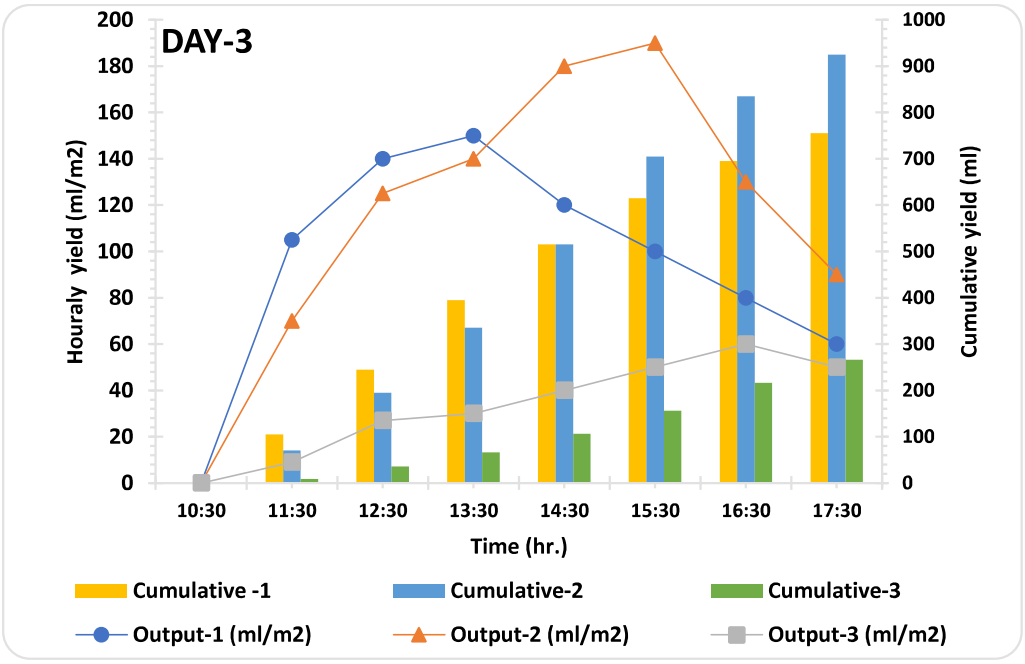

Figure 6. 9 Hourly variation of productivity during daylight time on Day-3

Figure 6.10 represents a comparative bar chart of cumulative yields of the three models that shows the suitability of a higher tilt angle in the winter season. The obtained result revealed that Model-2 performed better than other models. On the other hand, Model-3 gets the lowest solar insolation due to its east-west orientation and low tilt angle that makes it ineffective than other models although it creates the high basin water temperature but not able to yield high.

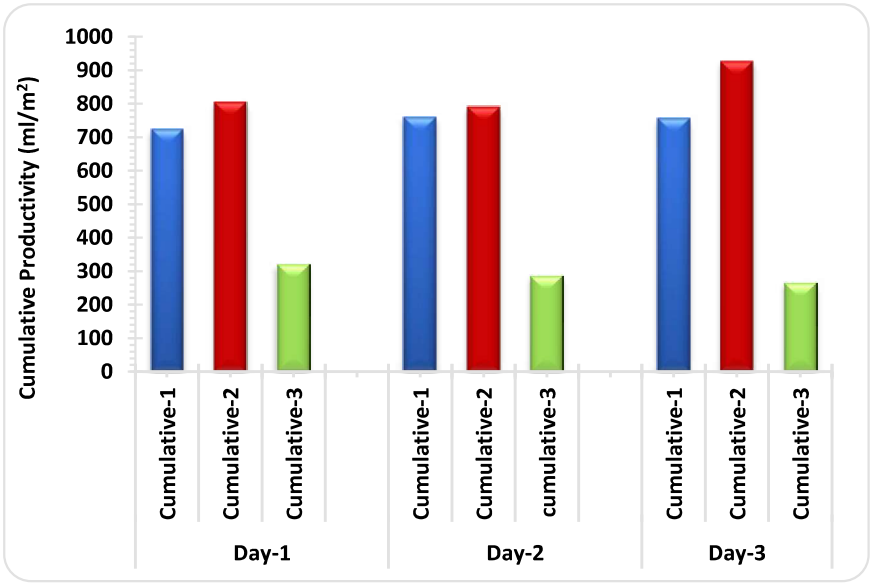

Figure 6. 10 Comparative analysis of day time cumulative yields of models on three days in winter.

6.2.3 Effect of wind velocity

Wind velocity is an important variable that influences the performance of SS. Wind blow provides a coolant effect to the condenser surface that increases the temperature difference and eventually boosts the SS output. The wind velocity profile shown in Figure 6.11 indicates that day-3 witnessed a high average wind velocity compared to day-1 and day-2 during the experiment, which helps to cool down the outer surface temperature of the glass cover by

liberating the latent heat of condensation. Figure 6.12 shows the average outer surface temperature that highlights the effect of wind velocity on day-3, which has a registered minimum temperature for all three models that eventually leads to higher yield.

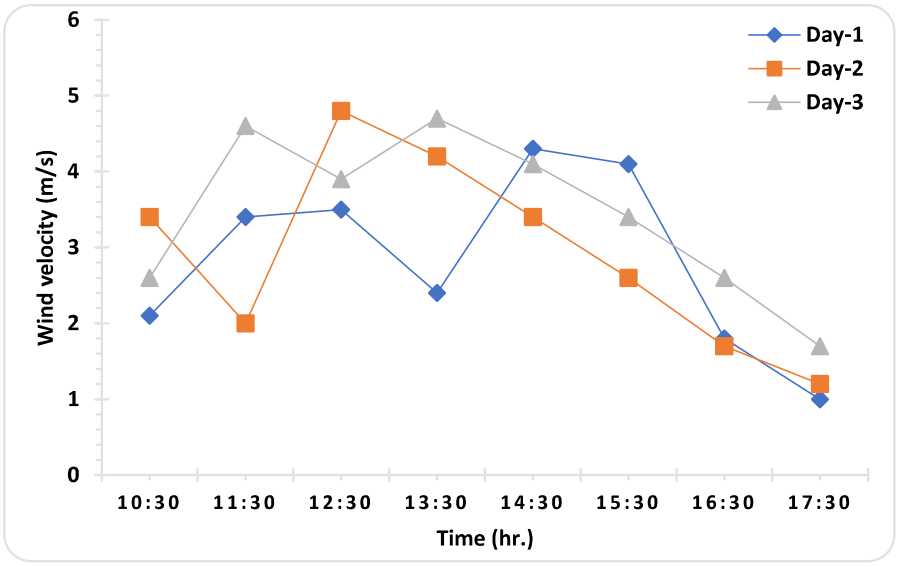

Figure 6. 11 Hourly variation of wind velocity

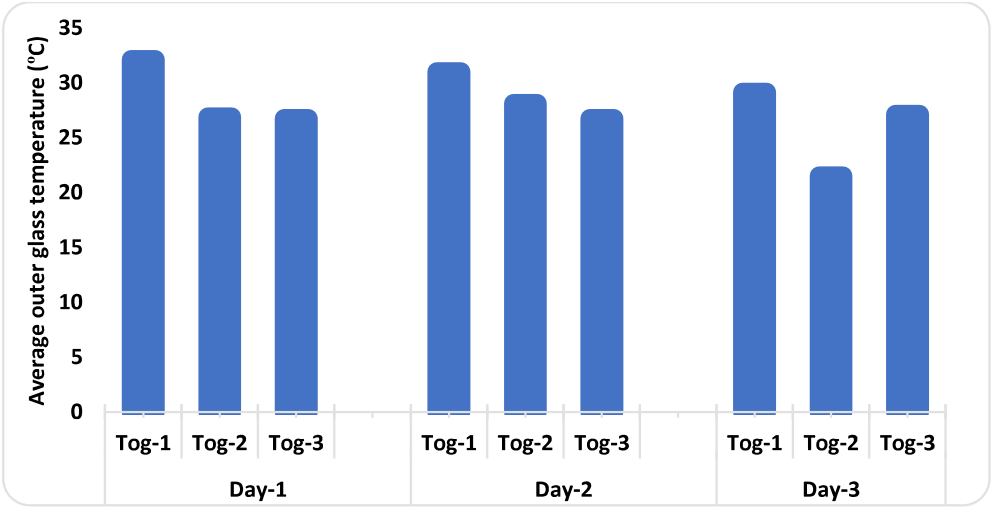

Figure 6. 12 Effect of wind velocity on the outer surface glass temperature of condenser cover

6.2.4 Nocturnal Productivity

Nocturnal productivity is a bonus output from solar still during this investigation. Model-2 has a better heat utilization factor during an off-sunshine period, as shown in Figure 6.13. Also, it has a favorable tilt angle that facilitates condensate flow to the trough, making it more efficient in both day and night conditions. The nocturnal yield of these models was investigated from 17:30 to 10:30 on the next day and revealed that in this period again, Model-2 provided a maximum yield of 735 mL/m2 as compared to 435 mL/m2 and 275 mL/m2 for Model-2 and Model-3 respectively on different days. During the sunshine period, the heat-retaining capacity of fabricating material (Fiber reinforcement plastic) is promising as that serve as the source of heat for basin water at night. The nocturnal period is considered from 17:00 hr. to 10:00 hr. (time interval of 17 hrs.). During this, the glass surface was also covered with an insulating cover (polystyrene) on all models that prevented any heat loss from the glass cover. That helps maintain the good temperature difference between basin water and glass cover that eventually boost the yield at night.

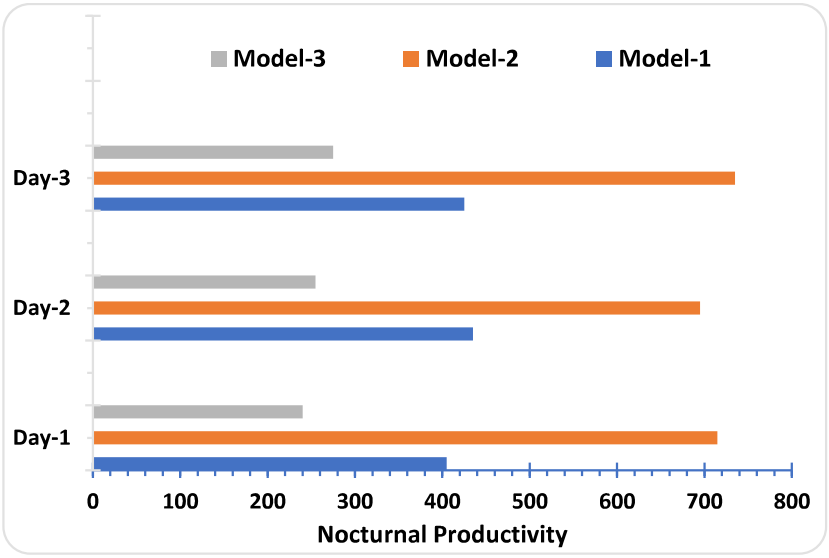

Figure 6. 13 Nocturnal productivity of solar stills

6.3 Efficiency comparison

6.3.1 Thermal Efficiency

The efficiency for conventional rooftop solar still is defined as the ratio of total heat utilized during the evaporation of basin water to the total solar energy that falls on the basin area [125]. Efficiency does not include nocturnal yield because sunlight is available in daylight only. The efficiency of model-1 and model-2 are calculated by Eq. (1) as follow [126] came nearly the same as illustrated in Figure 6.1. On day-2 performance of SSs was better than other two days due to good average solar flux condition of 416, 456, 372 W/m^2 and heat retaining capacity. Besides this, model-3 showed minimum efficiency due to low trapping of solar flux and backdrop of condensate into the basin. The outcomes of the experiments are tabulated in Table 6.1.

$$\eta = \frac{\Sigma \dot{m}_e L_{fg}}{\Sigma I(t)s \times A_s \times 3600} \ldots\ldots\ldots\ldots\ldots\ldots\ldots\ldots\ldots\ldots \quad (1)$$

Here, $\dot{m}_e$ is yield (kg/h), L_{fg} is average latent heat (kJ/kg) at basin water temperature (T_w in °C), I(t) is the solar radiation (W/m^2), and A_s is absorber surface area (m^2). Average latent heat can be calculated from Eq. (2) as follow [127].

$$L_{fg} = 10^3(2501.9 - 2.40706T_w + 1.192217 \times 10^{-3}T_w^2 - 1.5863 \times 10^{-6}T_w^3) \ldots\ldots\ldots\ldots\ldots\ldots\ldots\ldots (2)$$

Table 6. 1 The productivity and efficiency of models on different days.

Yield (mL/m^2) →	**Day-1**		**Day-2**		**Day-3**		
	Daytime	Nocturnal	Daytime	Nocturnal	Daytime	Nocturnal	**Max. Efficiency**

Model-1	722	405	760	435	755	425	17.15 %
Model-2	805	715	792	695	925	735	17.25 %
Model-3	320	240	286	255	266	275	7 %

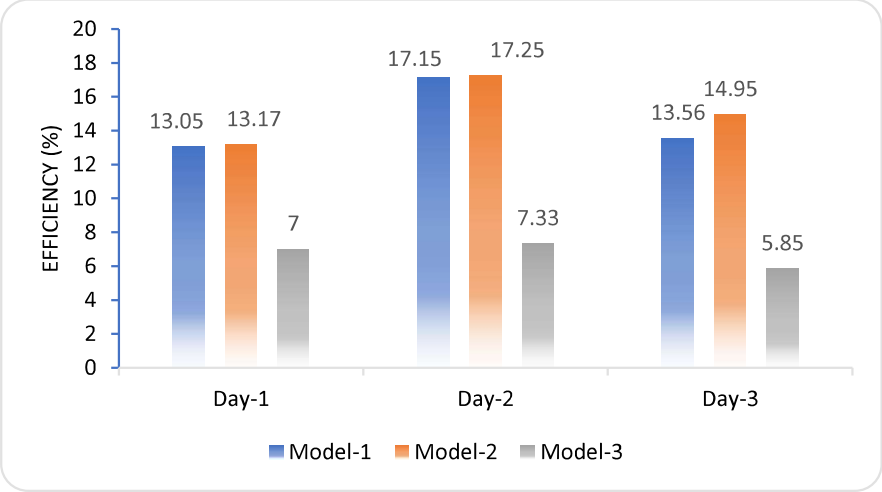

Figure 6. 14 Efficiency variation of models on three different days

- *Heat loss:*

Due to low efficiency of solar still, large amount of solar energy lost which is calculated from Eq. (3).

$$Q_{S,h} = 3600 \times A_s \times I(t)$$

$$Q_{lost,h} = (1 - \eta_h) \times Q_{S,h} \ldots\ldots\ldots\ldots\ldots\ldots\ldots\ldots (3)$$

On day-2, heat lost from model-1, 2, and 3 were 1240 kJ, **1358 kJ** and 1241kJ per hour respectively. Comparing, heat loss from the unit predicted from the theoretical model as given by Eq. 20.

$$Q_{loss} = A_{bs} U_i (T_{ins} - T_{amb})$$

The overall heat transfer coefficient (U_i), neglecting radiative heat transfer coefficient, free

convective heat transfer coefficient in ambient condition is in the range of 5-25 W/m^{2}K. Taking 13 W/m^{2}K for calculation, insulation temperature of 35°C and ambient temperature of 28°C. Model-2 has surface area of 2.35 m^2 (Table 3.1),

$$Q_{loss} = 2.35 \times 13 \times (35 - 28) \text{ W/m}^2$$

$$= 213.85 \text{ J/s} \times 3600 \text{ s}$$

$$= \mathbf{769.86 \text{ kJ.}}$$

As a result, the experimental results showed a 1358 kJ heat loss, whereas the theoretical calculations show a 769.86 kJ heat loss from the insulating side. That suggest heat loss form glass wall will be around 588 kJ.

6.3.2 Exergy analysis

The exergy analysis is the qualitative analysis based on second law of thermodynamics. It can be calculated by Eq. (4), by calculating the total exergy received in term of solar energy (Eq. 6) and total exergy output in term of distillate produced (Eq. 5), [128]

$$\eta_{Ex} = \frac{Ex_{out}}{Ex_{in}} \dots\dots\dots\dots\dots\dots\dots\dots\dots\dots\dots\dots\dots\dots\dots\dots (4)$$

Ex_{in} is the maximum available energy (exergy) received from the sun, Eq. 6, and Ex_{out} is the total exergy out from the solar still in the form of distilled water, Eq. 5, compared to ambient condition.

$$Ex_{out} = \frac{\dot{m} L_{fg}}{3600}\left(1 - \frac{T_a}{T_w}\right) \dots\dots\dots\dots\dots\dots\dots\dots\dots\dots\dots\dots\dots (5)$$

$$Ex_{in} = I_s A_b \left(1 - \frac{4T_a}{3T_s} + \frac{1}{3}\left(\frac{T_a}{T_s}\right)^4\right) \dots\dots\dots\dots\dots\dots\dots\dots (6)$$

Here T_s is the sun's surface temperature taken as 6000 K, T_a is ambient temperature (K), T_w is basin water temperature (K), 'I_s' is solar flux (W/m^2).

The calculation showed that model-2 performs better than other models regarding exergy efficiency. Model-2 achieved 1.1% exergy efficiency compared to model-1 and model-3, which achieved only 0.6% and 0.3% in the winter season, as shown in Figure 6.15.

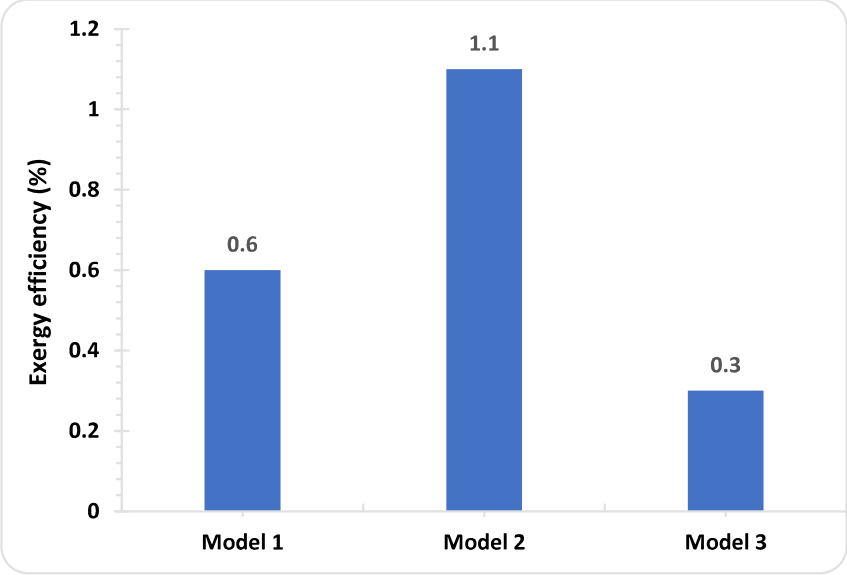

Figure 6. 15 Exergy efficiency of all three model

6.3.3 Effect of tilt angle

Glass cover tilt angle has a great impact on SSs which is found in current experimental investigation. The effectiveness of SS greatly depends on this tilt angle in the winter season. Model-1 which has 25° from horizontal southward facing has three days average distillate of 1167 mL/m^2 and model-2 which has 30° from horizontal southward facing has an average distillate of 1555 mL/m^2 in 24 hours at the geographical location of Varanasi (25.2623°N) in composite climate of India. Being in the northern hemisphere, in the winter season altitude (inclination) angle decreases as the sun apparently displaced toward the south.

6.4 Effect of BPQD concentration on SS

6.4.1 Variation of climatic condition

The effect of ambient condition is very significant in solar desalination process. Breeze with good solar radiation is most desirable condition for good performance of solar still. To perform the experiment two identical solar stills are designed and fabricated to investigate the effect of Pyrex glass quantum dot concentration on solar still. To do so four concentrations of Pyrex glass viz. 0g, 5g, 10g, 15g was mixed with 500 mL of black dye. The experiment was performed on several days although present article provides two days data. These two days have almost similar environmental condition as compared in Figure 6.16. The average solar radiation and ambient temperature on day-1 was 481.6 W/m^2 and 34.9ºC as compared to day-2 was 475.1W/m^2 and 35.7ºC. On day-1, solar still with 0gand 5g QD were investigated and on Day-2, solar still with 10g and 15g QD were investigated. Similar type of environmental condition allows to compare the results of two days.

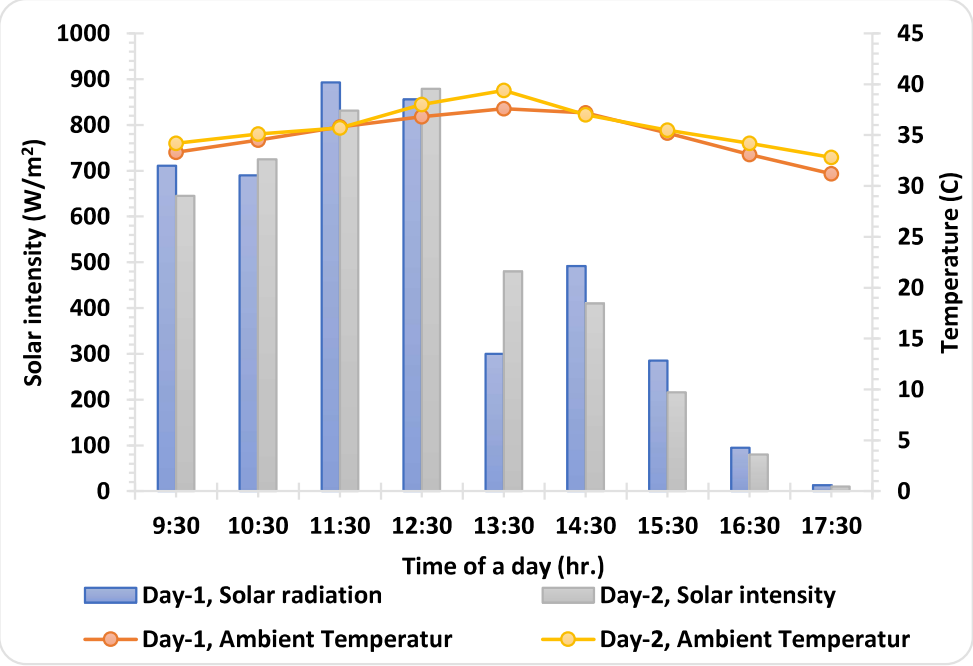

Figure 6. 16 Solar radiation and ambient temperature variation.

6.4.2 Hourly variation of T_{bw} and T_{ig}

Figure 6.17 Showed the hourly temperature variation of basin water and inner glass in all four concentrations. With homogeneous mixing of black phosphorus quantum dot (BPQD) in black dye improve the heat absorption capacity that is reflected by basin water temperature increase. It was found that with 0g (without QD) black dye raised the basin water temperature reached up to 51ºC only. Whereas, the maximum temperature with QD reached up to 55ºC, 60ºC and 68ºC with 5g, 10g and 15g concentration. Also, the maximum temperature is achieved at 13:30 after the peak solar intensity that indicate high heat capacity of basin water and sudden change in solar intensity near observation point. The rate of increase in temperature of basin water is maximum of 5.25 ºC/hr. in case of 15g QD as compared to 4 ºC/hr., 3 ºC/hr. and 2 ºC/hr. in case of 10g, 5g and 0g QD concentration. The inner glass temperature was also increasing as QD concentration increases which was due to large heat accumulation inside solar basin due to greenhouse effect. The temperature difference between basin water and inner glass temperature is the driving force of solar desalination. By the use of basin temperature increases significantly compared to inner glass surface temperature that eventually boost the yield. Conventional solar still without QD able to create average temperature difference of 3.47ºC while with 15g QD reached 7.33ºC. That highlights the improvement in heat absorption capacity of absorber surface and side walls of still by the application of QD.

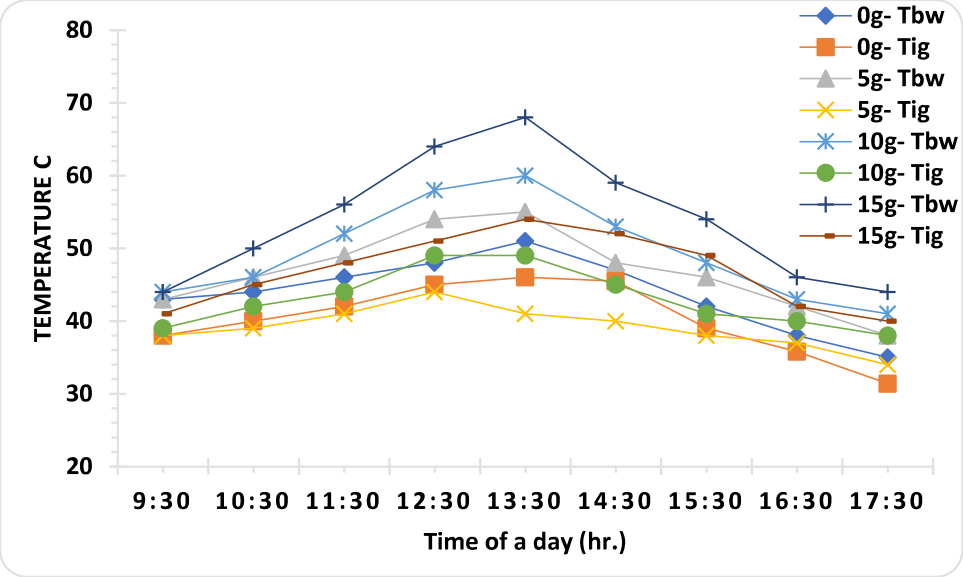

Figure 6. 17 Hourly variation of basin water and inner glass cover temperature with different concentration of pyrex glass

6.4.3 Experimental and Theoretical Comparison

Theoretical modelling is also developed to investigate the performance of solar stills with different concentration of QD under different assumptions and conditions. Figure 6.18 indicate the average basin water temperature in theoretical and experimental condition that facilitate to compare the deviation of theoretical results with experimental observations. Compared to experimental observations, theoretical result of average basin water temperature deviate from 2.28% for 0g QD to 6.2% for 15g QD. This deviation occurs due to some assumption like leak proof fabrication and no heat loss from side walls taken during mathematical modelling and its magnitude increasing with high heat accumulation inside basin. The standard deviation error bars are also used to show the variability. Long error bar lines are indicating the large variation of temperature from its average value whereas short error bars indicate less variation from its average value as shown in Figure 19. It also

highlights the increase in basin water temperature with increase in concertation it also showed the variation of theoretical basin water temperature with time and compare it with experimental observations for 0g, 5g, 10g, and 15g QD concentration condition.

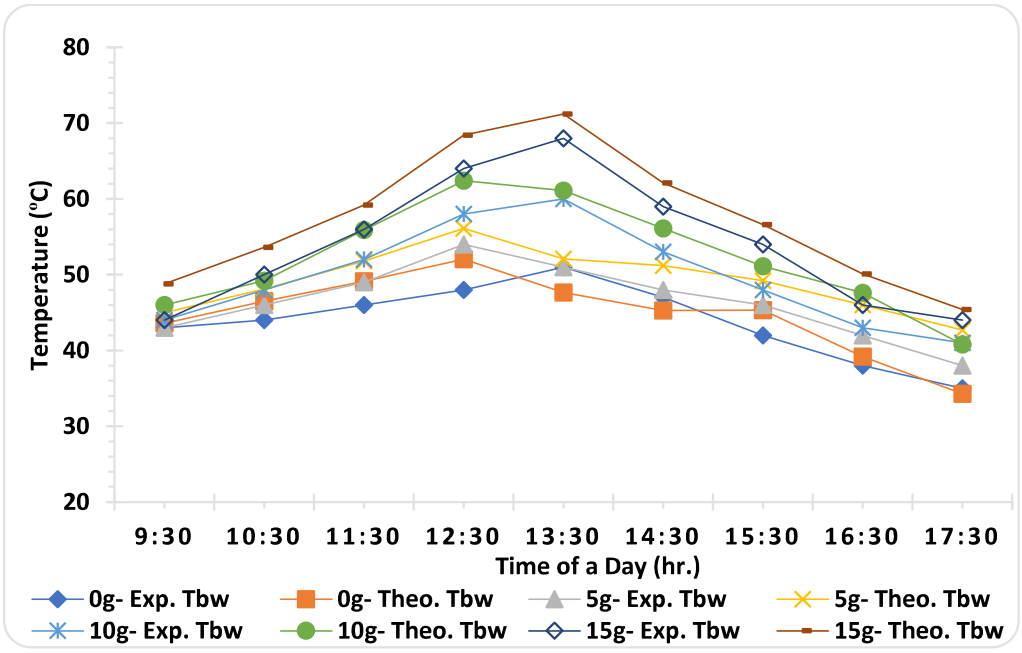

Figure 6. 18 Experimental and Theoretical variation of basin water

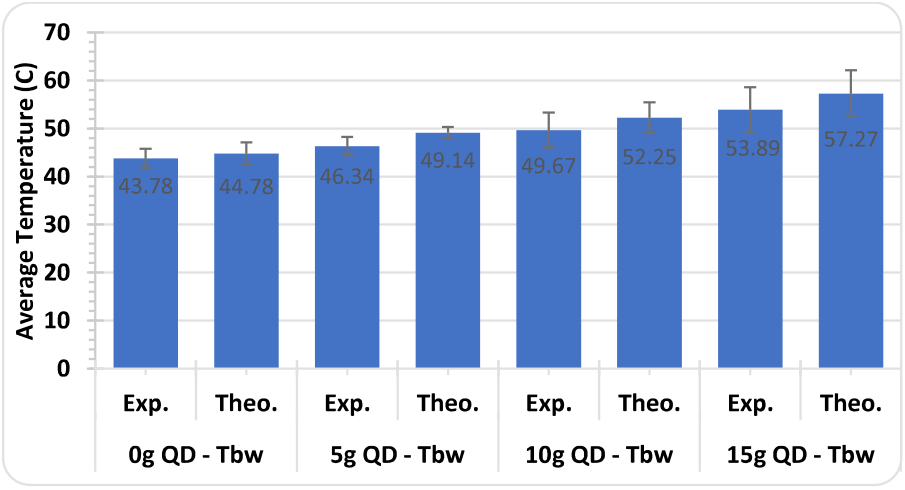

Figure 6. 19 Variation of average basin water temperature in experimental and theoretical condition

6.4.4 Yield of solar stills

Solar still yield varied significantly by increasing the concentration of QD. Figure 6.20 present the distilled water yield with time with different QD concentrations. Both experimental and theoretical yields are shown simultaneously to validate the theoretical modelling. Solar intensity remains highest at 11:30 to 12:30 during this period yield is maximum. Solar still with 15g QD, produces 460 mL and 481mL experimentally and theoretically. Similarly, with 10g, 5g and 0g QD maximum yield reached up to 380.46 mL and 370 mL; 303 mL, 260 mL; and 230 mL, 237 mL theoretically and experimentally respectively. On Day-1, at 13:30 solar intensity falls yet yield increases, this may be due to fall of solar intensity occur near observation point and hence the effect of this become apparent at 14:30 in the form of low yield. Whereas, on Day-2, this solar intensity falls gradually during 12:30 to 13:30 that affect the performance and become apparent at 13:30 with low yield. As quantum dot concentration increases, the absorption property of FRP material improves, resulting in a rapid rise in the temperature of the basin surface, which increases the Rayleigh number. Thus, the convective heat transfer coefficient increases from the basin surface to water as per Eq. no., ultimately improving the unit's productivity. Furthermore, based on experimental observation, a rise in concentration is believed to enhance the absorptivity value. This serves as the foundation for a theoretical examination of solar still coated with QD. In this investigation, the uncertainty value is calculated, which was found to be under the limit. However, a good yield match at higher concentrations of QD indicates that the assumptions made agree with the physical environment satisfactorily.

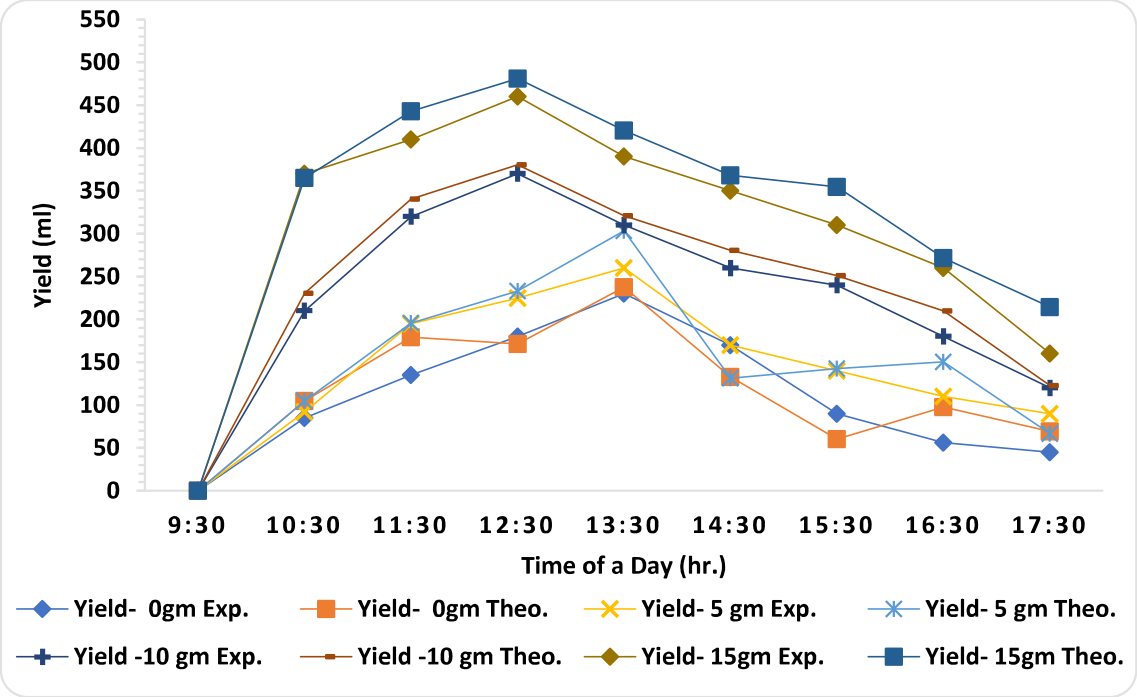

Figure 6. 20 Hourly variation of distilled water yield in different QD concentration

QD materials are used in this investigation to improve the solar still productivity. It is used to increase the radiative properties of the basin surface; however, it also broadens the range of the solar absorption spectrum, which is witnessed by the rise in basin surface temperature. That results in the rise of basin water temperature, and eventually raising solar still's productivity with an increase in QD concentration in black dye. Mathematical modeling is done based on classical physics because it incorporates the influence of quantum dot material in terms of absorptivity and heat transfer coefficient from basin surface to basin water.

Figure 6.21 shows the cumulative yield of solar still in experimental and theoretical mode with different concentration of QD. Theoretical modeling is performed to generalized the condition in tropical climate of India. The theoretical results are validated by experimental results that shows 6.1%, 3.58%, 6.20%, and 7.66% deviation with 0g, 5g, 10g, and 15g case.

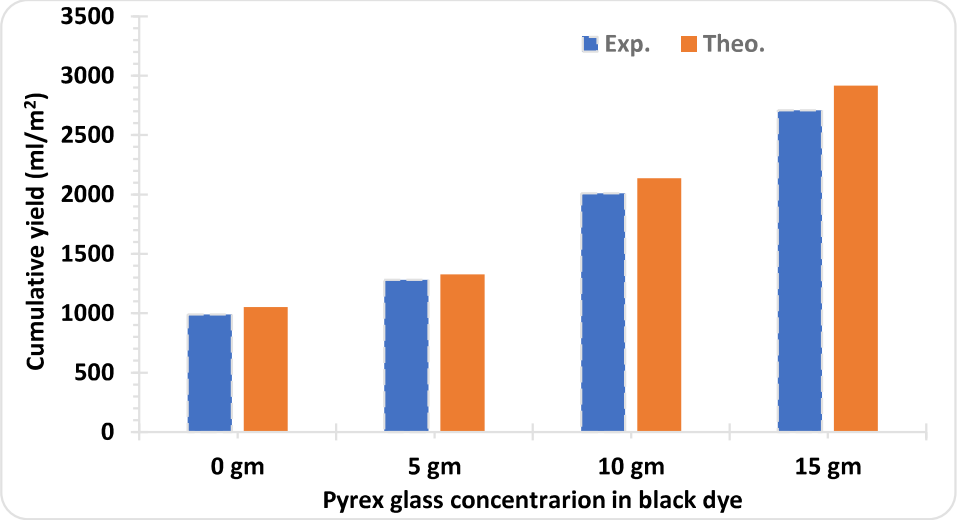

Figure 6. 21 Cumulative yield from solar stills at different concentration of Pyrex glass in 500 mL of black dye

There was discrepancy between the experimental and theoretical distillate output results. This occurred because

1) In theoretical modeling, it was assumed that the setup was completely insulated, no vapor leakage, dropwise condensation occurs but it is not possible in true sense.

2) Secondly, solar intensity, temperature of the water and glass, and wind velocity would remain constant for 1 hr. implies that time constant was 1 hr. for this experiment, however solar intensity changes at any moment owing to changes in the sun's position, as well as meteorological conditions.

With all assumptions made, mathematical modelling became possible, resulting in theoretical distillate production in this study that was comparable to experimental distillate output. The theoretical study forecast of the distillate output with a maximum variation of experimental distillate output of about 7.67%.

6.4.5 Effect of wind on Convective HTC

Although glass surface temperature controlled by solar flux condition but it is also influenced by wind velocity dictated by convective HTC empirical formula. The convective HTC from glass to air is an important parameter to cool down the condenser surface. The free convective heat transfer coefficient of air varies from 2.5 to 25 W/m^{2}K in zero wind velocity condition. During the course of experiment wind velocity varies from 1.8 to 4.8 m/s and corresponding to that convective HTC varied from 8.2 to 17.2 W/m^{2}K in case of SS coated with 15g QD.

Wind velocity has significant effect on heat removal from outer surface of glass. The free convective heat transfer coefficient of air can vary from 2.5 to 25 W/m^{2}K. There were various investigations that results two empirical relations [129] that provide convective heat transfer coefficient.

$$h_{conv.\ g-air} = 2.8 + 3V \qquad 0<V<7\text{……..(7)}$$

$$h_{conv.\ g-air} = 5.7 + 3.8V \qquad 0<V<5\text{……(8)}$$

Equation (8) gives the overall heat transfer coefficient considering convection and radiation whereas, equation (7) gives only convective heat transfer coefficient over inclined glass surface in natural convection condition. In present experiment average wind velocity during course of experiment was around 3 m/s corresponding to this $h_{conv.\ g-air}$ will 11.8 W/m^{2}K by equation (7).

With increasing the QD concentration temperature difference between basin liner and basin water increases ($\Delta T_{b\text{-}w}$). Effect of QD concentration on SS's convective heat transfer coefficient from basin to water ($h_{conv.\ b-w}$) can be analyzed by Eq. (9),

$$h_{conv.\ b\text{-}w} = C \times (K/L) \times [Gr \times Pr]^{1/n} \quad \ldots\ldots\ldots\ldots\ldots\ldots\ldots\ldots (9)$$

Eq. (7) shows ($h_{conv.\ b-w}$) function of Grashof No. (Gr) which is function of $\Delta T_{b\text{-}w}$. Hence, with increase in QD concentration Gr No. increases with that $h_{conv.\ b-w}$ also increase.

From water to glass different heat transfer coefficients also increases due to increase in basin water temperature as Eq. (10), (11), and (12).

$$h_{g\text{-}w} = h_{\text{radiation, g-w}} + h_{\text{convection, g-w}} + h_{\text{evaporation, g-w}}$$

$$h_{\text{radiation, g-w}} = \varepsilon_{\text{effective}}\ \sigma\ (T_w^2 + T_g^2)\ (T_w + T_g) \quad \ldots\ldots\ldots\ldots\ldots\ldots\ldots\ldots\ldots\ldots\ldots\ldots\ldots\ldots (10)$$

$$h_{\text{convection, w-g}} = 0.884[T_w - T_g + (P_w - P_g) \times T_w/(268.9\times10^3 - P_w)]^{1/3} \quad \ldots\ldots\ldots\ldots\ldots (11)$$

$$h_{\text{evaporation, w-g}} = 16.276 \times 10^{-3} \times h_{\text{convection, w-g}} \times \frac{P_w - P_g}{T_w - T_g} \ldots\ldots\ldots\ldots\ldots\ldots\ldots\ldots\ldots\ldots\ldots (12)$$

6.5 Efficiency comparison

6.5.1 Energy efficiency

During the sunshine, solar energy drives the desalination process inside the solar still. To assess the performance of solar still, solar still efficiency (first law efficiency) is a crucial parameter. According to the first law of thermodynamics, energy efficiency is the ratio of output energy (energy equivalent to distill water produced) to input energy (incident solar energy) in the same time duration.

6.5.2 Exergy Efficiency

The 2nd law of thermodynamics talks about the quality of heat energy and its maximum use relative to the dead state (ambient condition), which can be figured out by calculating the exergy efficiency. It can be defined as the ratio of maximum available energy (exergy)

received (E_{xin}) from the sun to the total exergy out from the solar still (E_{xout}) in the form of distilled water relative to the dead state.

Figure 6.22 compares solar still's thermal and exergy efficiency with different concentrations of QD in both experimental and theoretical conditions. The result showed maximum energy efficiency of 41.22%, 30.57%, 19.68%, and 15.21% with 15g, 10g, 5g, and 0g QD concentration. The higher efficiency of 15g QD concentration shows significant solar absorptance with the application of QD. However, theoretical energy was a bit higher at 44.37%, 32.49%, 20.39%, and 16.15%, respectively, relative to the experimental results due to some extreme assumptions taken during the modeling. Moreover, the exergy efficiency of SS was estimated as 2.75% and 2.71%; 1.41% and 1.57%; 0.84% and 0.92%; 0.50% and 0.68% for 15g, 10g, 5g, and 0g QD in case of experimental and theoretical condition. Exergy efficiency improves significantly with QD coating on SS due to increased heat absorption proportion relative to conventional SS.

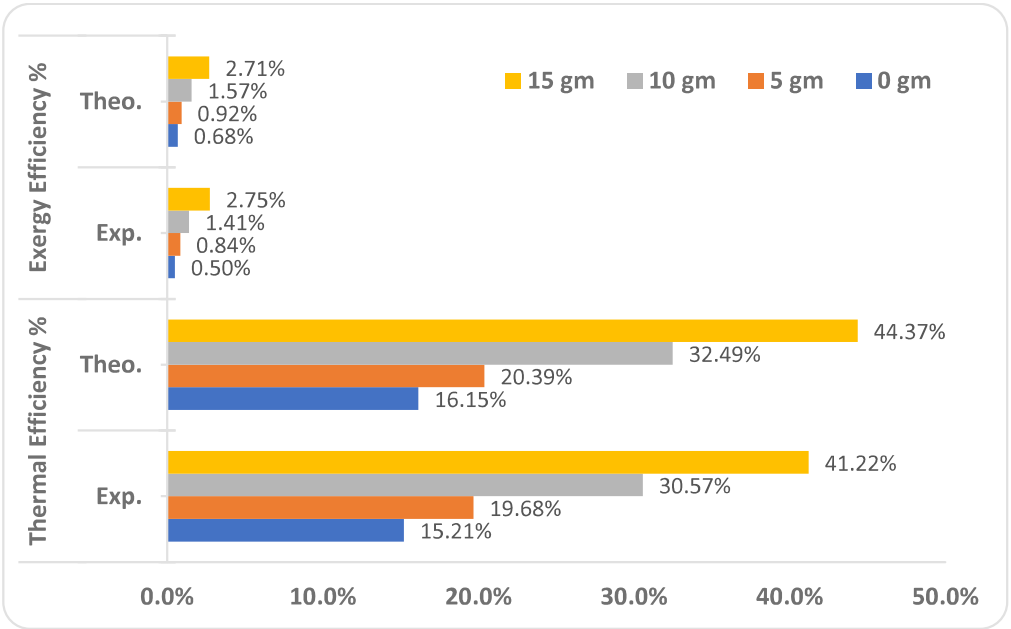

Figure 6. 22 Comparison of Thermal efficiency and Exergy efficiency on different

concentration of Pyrex glass in black dye

6.6 Performance of Prismatic SS

6.6.1 Conventional and Prism type SS

A Series of experiments have been conducted with Conventional and Prism-type SS without PCM and QD to observe the performance of the SS with respect to their yield and efficiency. Figure 6.23 highlights the temperature variation of basin water and inner glass surface temperature without using PCM and QD. High-temperature condition inside the basin drives the evaporation process more rapidly, although it negatively affects the condensation process on the glass surface. From a series of experiments, it was noticed that ambient temperature negatively impacts yield because it warms up the glass cover, reducing the condensation process rate. Also, PSS's end temperature condition indicates a comparatively fair heat retention capacity. The performance of SSs was not appreciable, but it sets the reference for further investigation.

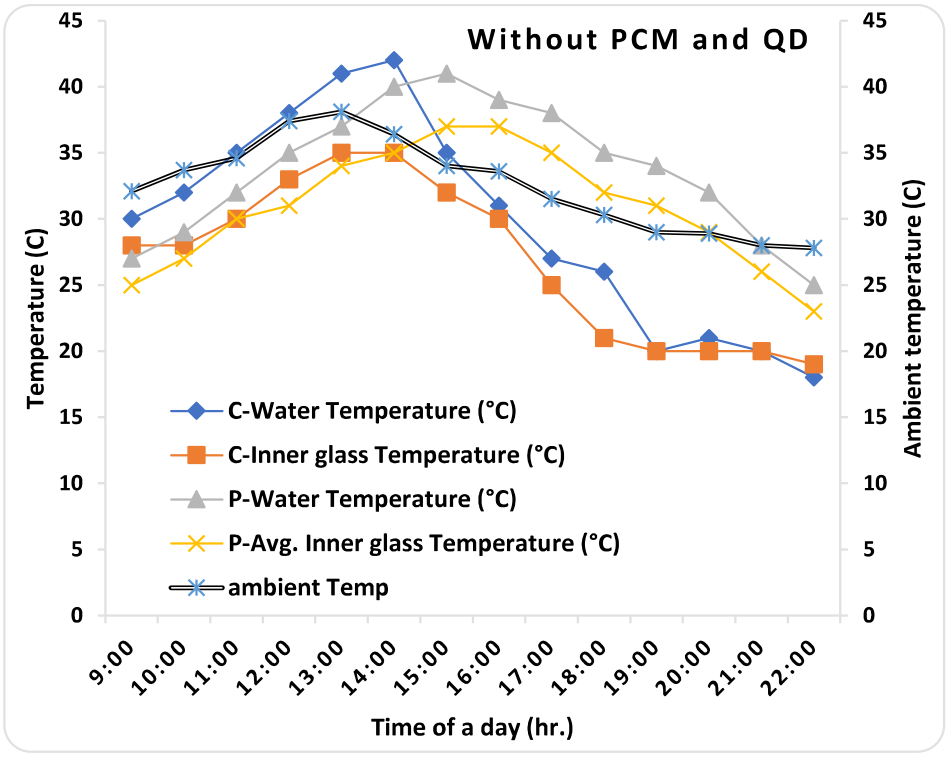

Figure 6. 23 Temperature variation of inner glass condenser surface and basin water with time

Figure 6.24 shows that Prism-type solar still (PSS) has a bit higher temperature difference (ΔT) between basin water and inner glass surface as compared to conventional solar still (CSS), initially, till 14:00 hr. CSS has able to maintain high ΔT compared to PSS. However, PSS could maintain its ΔT for a more extended period than CSS at high temperatures. After sunset, negative ΔT indicates inner glass surface temperature becomes higher than the basin water temperature. However, maximum ΔT reached up to 8°C in the case of CSS as compared 5°C in the case of PSS, but PSS was able to maintain a higher average ΔT as compared to CSS during 13 hrs. of working period.

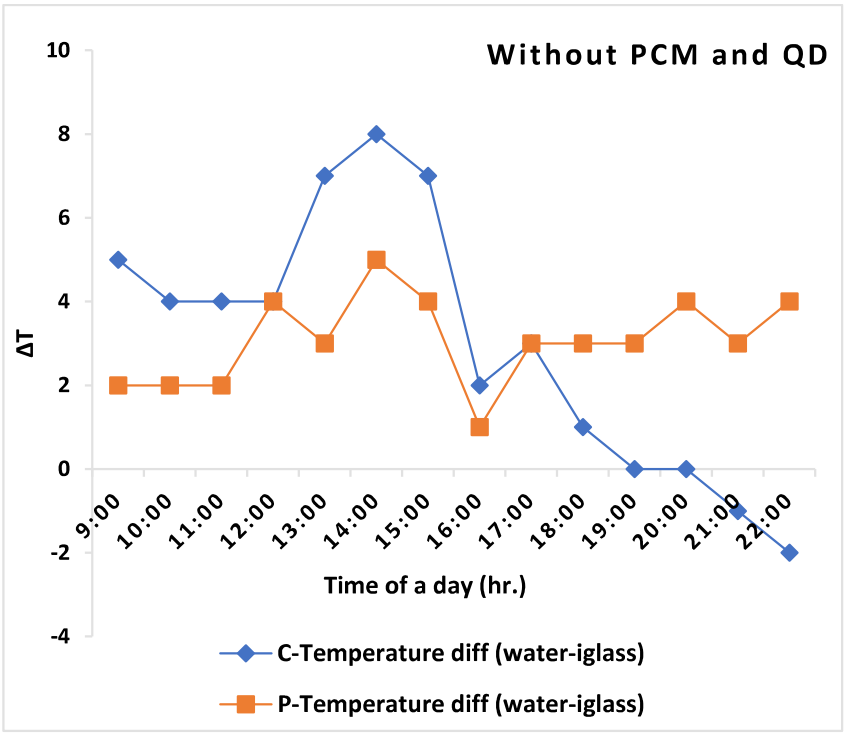

Figure 6. 24 Variation of change in temperature difference (ΔT) between inner glass condenser surface and basin water with time

Figure 6.25 shows the distilled water yield with respect to time and the effect of solar flux radiation on yield. PSS has a double slope arrangement and a small side glass coverage area. PSS has a more solar entrance area relative to CSS, instead of that, solar radiation capture was less. In similar climatic conditions, average solar radiation acceptance was 437 and 371W/m^2 for CSS and PSS, respectively. It also shows that the hourly yield of PSS is higher than CSS after 15:00 hr., which eventually makes a higher cumulative yield for PSS of 1830 mL than CSS of 1660 mL/m^2. This total cumulative yield (sunshine yield and after sunshine yield) lead was obtained after the sunshine period, showing that PSS has better heat retention capacity than CSS.

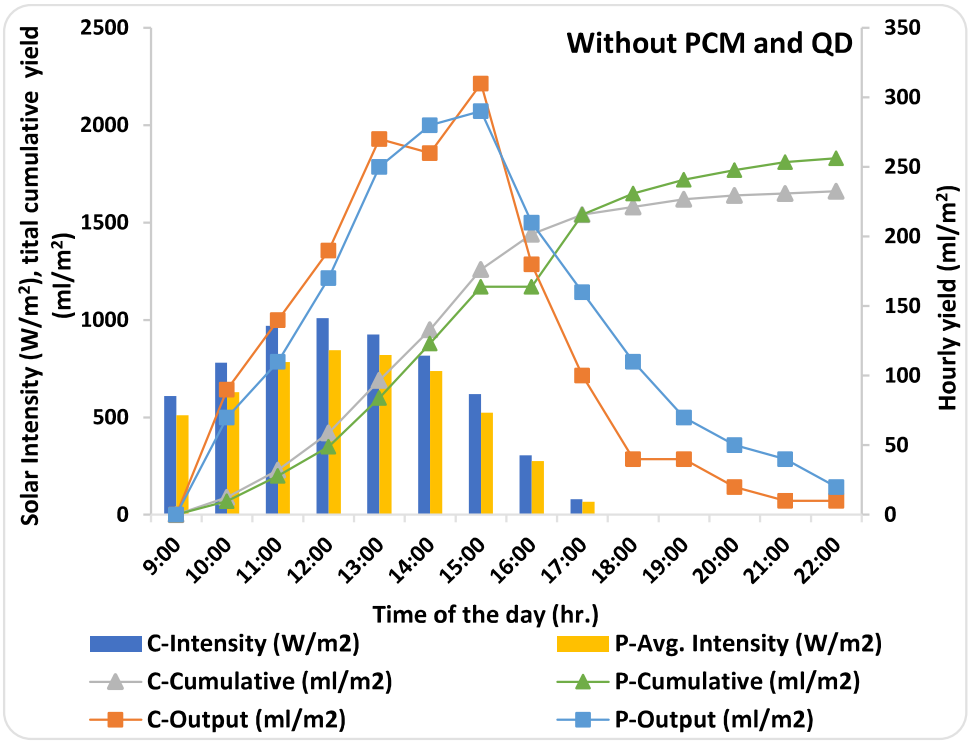

Figure 6. 25 Variation of hourly yield, total cumulative yield, and solar radiation intensity with time

6.6.2 Effect of PCM on Conventional and Prism type SS

After completing the first stage of the experiment, the second stage was initiated to observe the performance of solar still with PCM only. PSS with PCM performs well in sunshine and off-sunshine periods relative to CSS with PCM. Figure 6.26 shows basin water temperature in case CSS reaches higher than PSS in the sunshine period, although this gets reversed in the off-sunshine period. After sunset, the PSS basin water temperature was higher than CSS. The temperature difference between basin water and inner glass surface (ΔT_{wg}) was also higher in the case of PSS, as shown in Figure 6.27. During the off-sunshine period (after sunset), PSS was able to maintain a higher average temperature difference (ΔT_{wg}) of 4.83ºC as compared to CSS that, of 3.83ºC during the same period. In a day, CSS maintained ΔT_{wg}

at 5.28°C compared to 6.42°C for PSS. This temperature difference led to enhance the rate of yield.

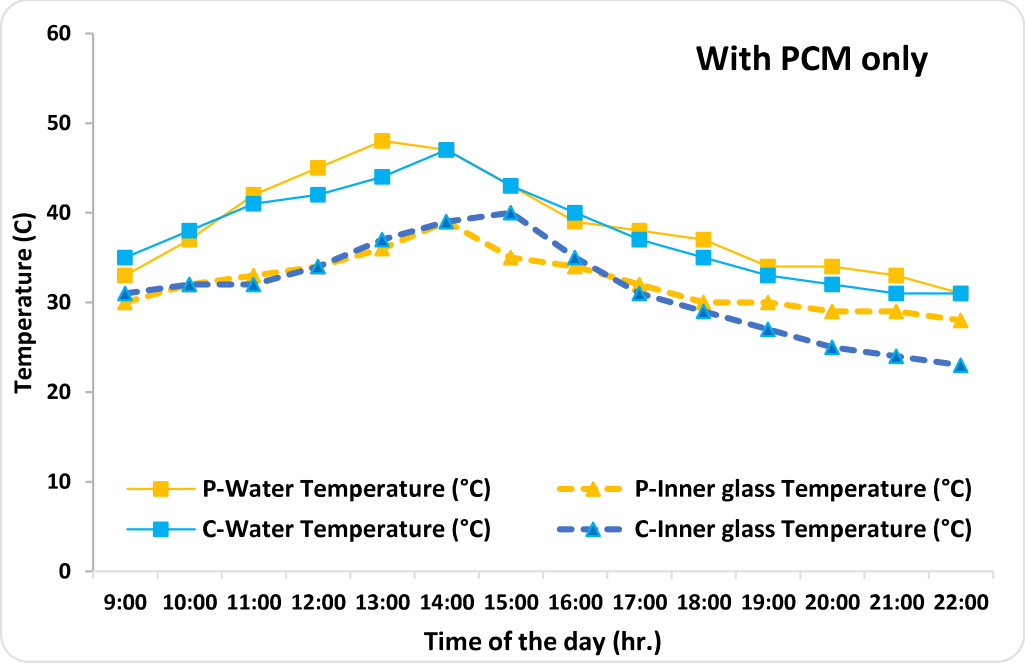

Figure 6. 26 Temperature variation of inner glass condenser surface and basin water with time

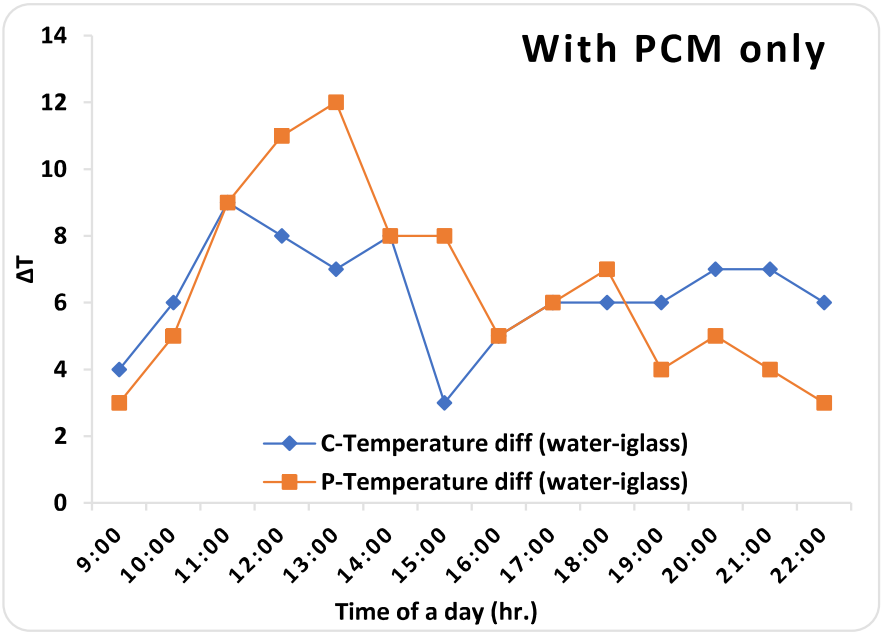

Figure 6. 27 Variation of change in temperature difference (ΔT) between inner glass condenser surface and basin water with time

Lauric acid (PCM) has good heat storage capacity and performs well with PSS. Because of its non-toxic nature, it can be used with minimal precaution. During this investigation, lauric acid could store the heat up to 39°C and 40°C with CSS and PSS. During the sunshine period, PCM gets charged, as represented by blue bars. During charging, the basin water temperature was higher than the average PCM temperature. Although this charging mostly remains up to sensible heat storage level. After sunset, this stored energy gets utilized to heat the basin water, as shown by red bar lines, which is evident in both CSS and PSS, as shown in Figures 6.28 and 29.

Figure 6.28 represents the temperature variation of basin water and PCM with time in CSS, whereas, Figure 6.29 represents the temperature variation of basin water and PCM with time in PSS. By comparing these graphs, CSS basin water temperature did not rise effectively after sunset using stored energy that can be observed by the low average basin water temperature of 32.5°C relative to PSS of 34.5°C during the same period. Due to this, PSS performed slightly better than CSS arrangement, with ΔT_{wg} of 4.8°C and 4.2°C after sunset. PCM starts liberating heat after 17:00 hr. in both cases. Algebraic summation of the temperature difference between basin water and PCM can be termed as an 'Overall heat transfer factor' that was 12°C and 9°C in the case of PSS and CSS that suggest high-temperature gradient for PSS as compared to CSS represented by red bars after 17:00 hrs. Although the rate of heat transfer from PCM to basin water was nearly the same in both cases.

The physical significance of the overall heat transfer factor is the potential of heat transfer from PCM to basin water, which can be calculated by algebraic summation of the temperature difference between PCM and basin water during the heat transfer period. In sunshine conditions, the maximum temperature obtained by basin water in CSS was about 47ºC, whereas, in PSS, it reached up to 48ºC.

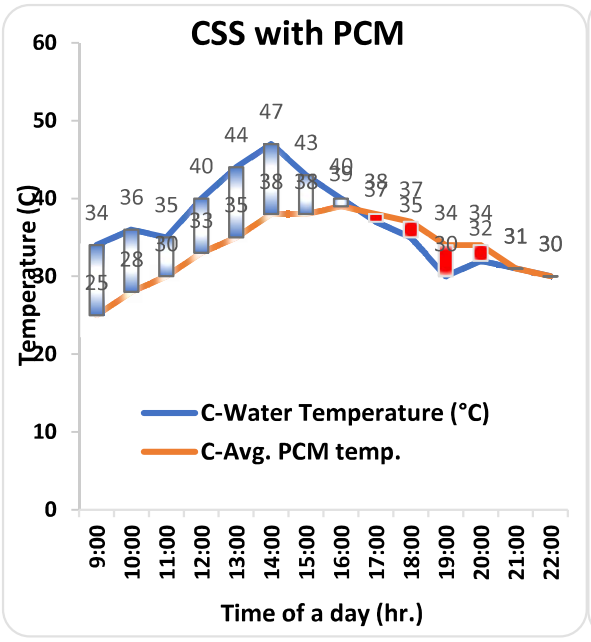

Figure 6. 29 Hourly temperature variation of basin water and PCM in CSS

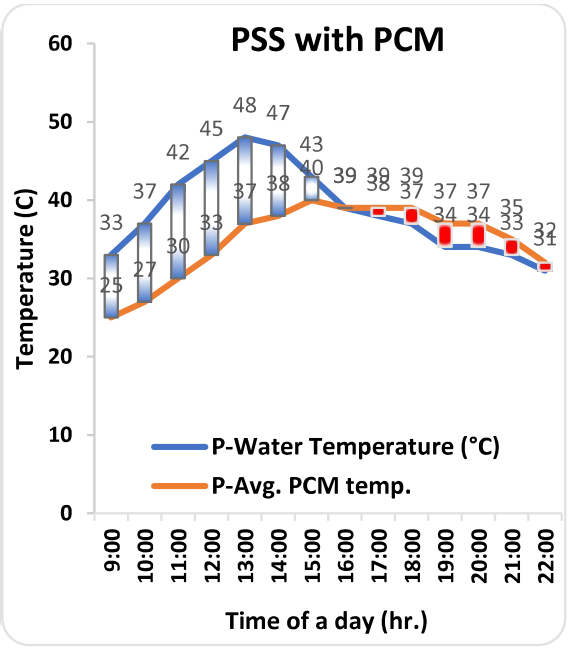

Figure 6. 28 Hourly temperature variation of basin water and PCM in PSS

Figure 6.30 represents the hourly and total cumulative yield (summation of yield) of distilled water from both CSS and PSS with PCM. The primary vertical axis presents hourly yield (mL/m^2), and the secondary vertical axis presents Solar Intensity (W/m^2) and total Cumulative yield (mL/m^2). Both solar stills perform well in sunshine periods, but after sunset, PSS yields higher than CSS, which is more due to its unique shape of solar still that does not allow to escape the heat from inside, which is common heat loss in CSS. The colder surface of the condenser facilitates the condensation phenomenon. However, to increase the

yield, evaporation should also get boosted, which is high in the case of PSS, making cumulative yield higher than CSS. Moreover, it shows the solar intensity variation with time, and precisely it represents the average solar radiation acceptance which was 429 and 361 W/m^2 for CSS and PSS, respectively, during the observation period. Yield increased by 38.25% and 42.16% compared to the previous case without PCM. Solar radiation condition was very much similar to the earlier set of experimental conditions on CSS and PSS without PCM.

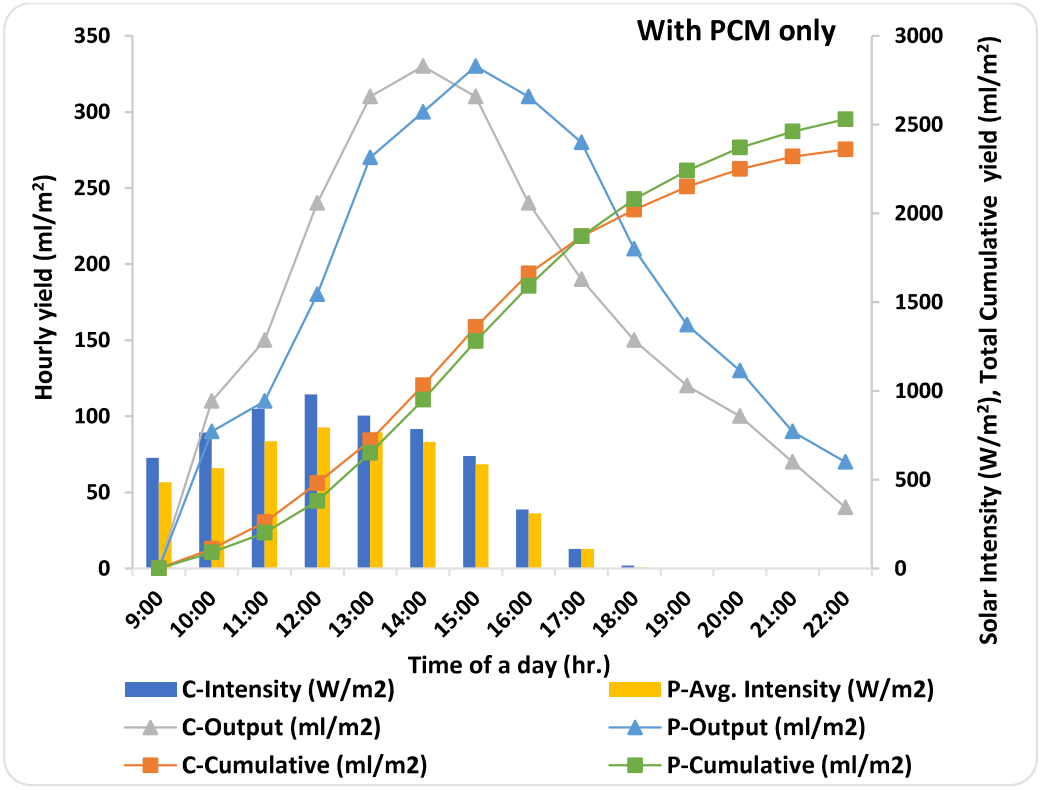

Figure 6. 30 Variation of hourly yield, total cumulative yield, and solar radiation intensity with time

6.6.3 Effect of QD and PCM on Conventional and Prism SS

A series of experiments were performed to examine the behavior of SSs with PCM and QD. Figure 6.31 shows the temperature variation of basin water and inner glass surface

temperature of both SS loaded with PCM and coated by black paint mixed with QD. It indicates the peak temperature of basin water reached up to 59ºC at 13:00 hr. in the case of PSS and 53ºC at 14:00 hr. in the case of CSS, which was higher than previous arrangements. However, it was noticed that the inner glass surface temperature was a bit higher in the case of PSS compared to CSS. In the case of PSS, the average inner glass surface reached up to 36.5°C, whereas with CSS, it was 35.9°C, creating adverse conditions for condensation.

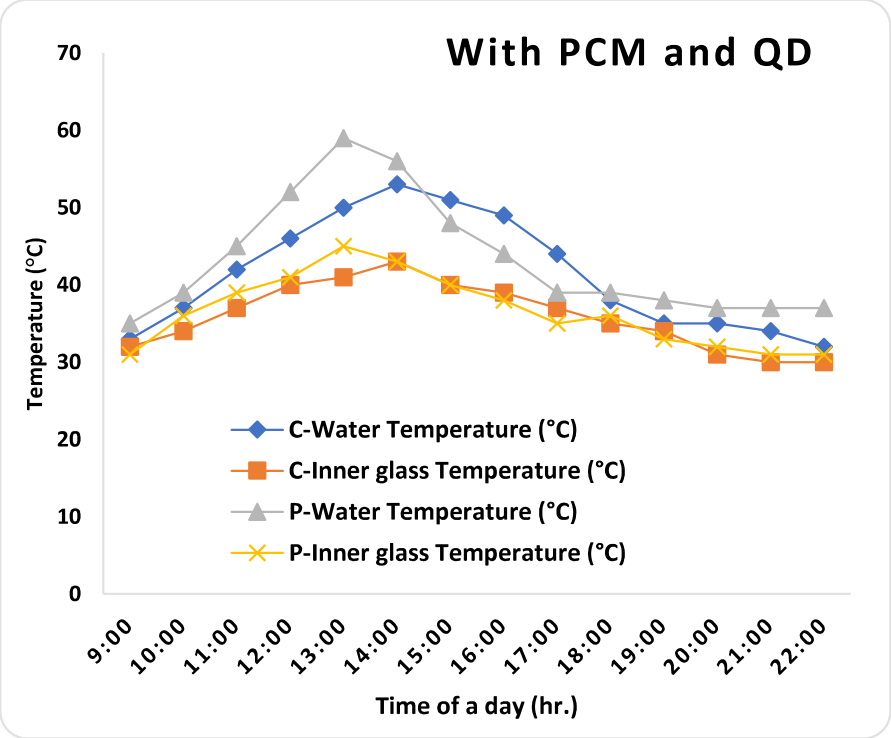

Figure 6. 31 Temperature variation of inner glass condenser surface and basin water with time

Figure 6.32 indicates the temperature variation of basin water and inner glass temperature (ΔT_{wg}), which highlights a rise in temperature difference compared to the previous case. In the previous case, the average ΔT_{wg} was 4.42°C and 3.83°C in the case of CSS during sunshine and off sunshine period that was improved to 5.42°C and 3.53°C in the same period. In the off-sunshine period, average ΔT_{wg} falls that indicate heat loss from basin water to

ambient bring down the average temperature of basin water. Whereas, in the case of PSS, in the previous case, ΔT_{wg} was 6.42°C and 4.8°C during sunshine and off sunshine condition that improves with QD material to 6.71°C and 4.83°C.

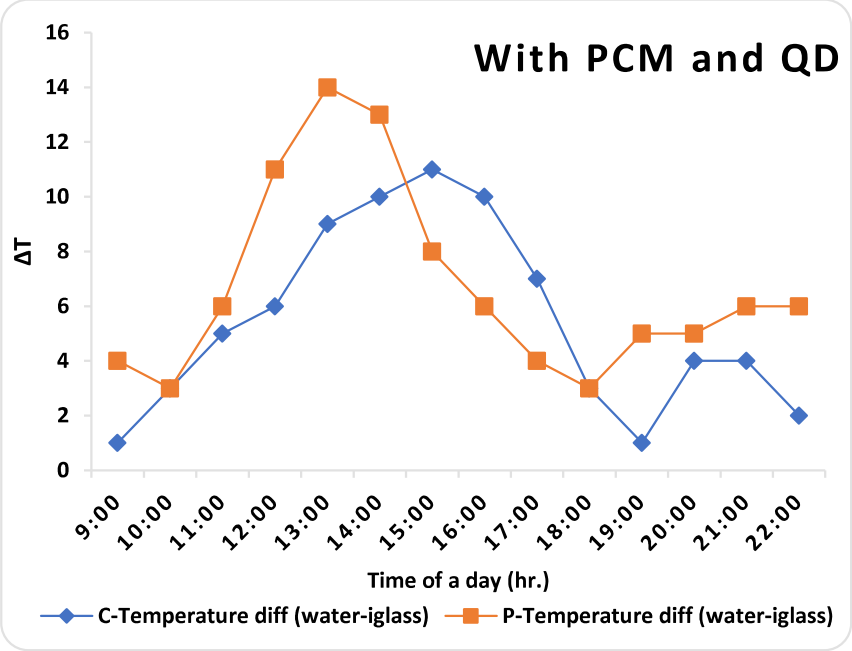

Figure 6. 32 Variation of change in temperature difference (ΔT) between inner glass condenser surface and basin water with time

Figures 6.33 and 6.34 represent the behavior of PCM's charging and discharging rate. After sunset, CSS could not transfer the heat effectively to the basin water compared to PSS, which can be attributed to the low water temperature compared to PSS at the respective time. In this case, the overall heat transfer factor (10ºC) for CSS and (23ºC) for PSS shows that using Q-dot material facilitates the PCM to transfer the heat to basin water with great potential. Also, the average basin water temperature remains high in the case of PSS (33.25ºC) relative to CSS (36.33ºC) using Q-dot material. Quantum dot material not only captures the extensive range of solar radiation but can also retain that heat for a more extended period, boosting the function of PCM. Figure 27 represents the hourly and cumulative yield and solar intensity

variation concerning time, showing that PSS is more effective. The graphs show that CSS can trap more solar radiation relative to PSS. Although cumulative yield is higher for PSS, this is due to the effective heat utilization (from PSS and CSS) susceptible to heat loss due to its inclined surface. Moreover, wind velocity becomes critical in the case of CSS because it facilitates condensation and allows heat to escape from the basin.

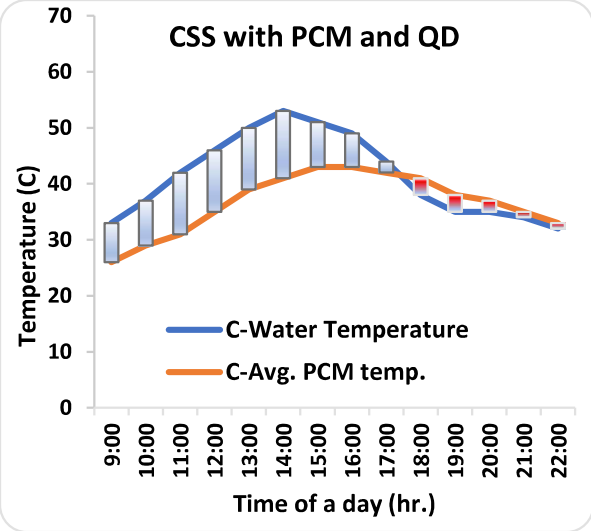

Figure 6. 33 Hourly temperature variation of basin water and PCM in PSS

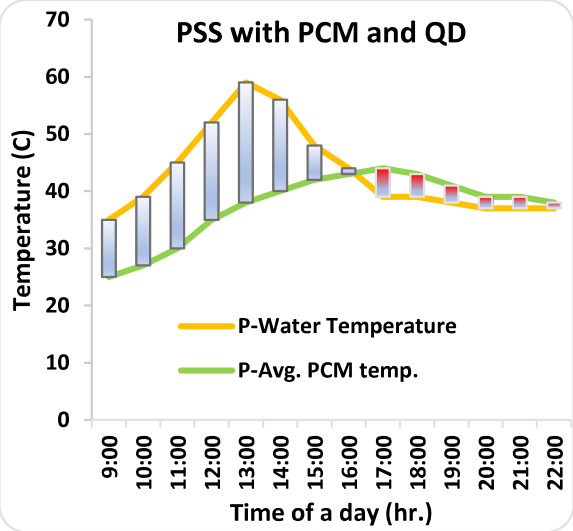

Figure 6. 34 Hourly temperature variation of basin water and PCM in CSS

6.6.4 Yield of modified solar still

Figure 6.35 represent the hourly yield variation on the primary vertical axis and the total cumulative yield on the secondary vertical axis with respect solar intensity of a day. Results suggest at 13:00 hr. PSS can produce a maximum hourly yield of 430 mL/m^2 compared to 400 mL/m^2 at 15:00 hr. Using PCM helps retain the heat energy that is eventually reflected by nighttime yield. Solar radiation was constantly higher in the case of CSS due to south facing design, whereas PSS could not capture that amount of flux, but its heat-retaining capacity was better. In this case, the total yield improved by 45.65% and 28.81% compared to the previous case. Concerning CSS of yield 3040 mL, PSS performed 21.21% better than

total yield of 3685 mL in 13hrs. span. Nocturnal yield shows significant improvement in this case. In the case of CSS, the yield reached 1110 mL, whereas, with PSS, the yield reached up to 1280 mL during the same period. It highlights the fact that QD was more effective during the sunshine period.

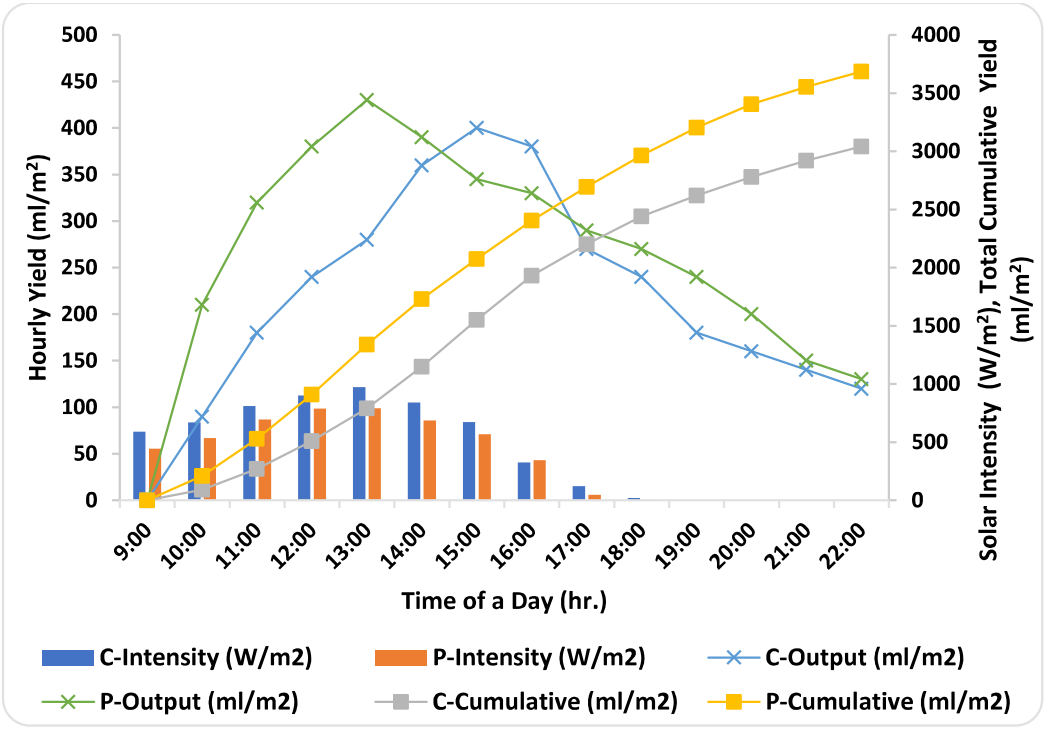

Figure 6. 35 Variation of hourly yield, total cumulative yield, and solar radiation intensity with time

6.7 Efficiency comparison

6.7.1 Utilization efficiency

During the sunshine period, solar energy is utilized to evaporate the basin water showing solar still's efficacy (first law efficiency). Hence, it can be defined as the ratio of energy equivalent to distilled water produced to the average solar intensity during working hours as Eq. (3). It can also be termed 'Indirect efficiency.'

$$Utilization\ efficiency\ (\eta_u)$$

$$= \frac{Energy\ required\ for\ distilled\ water\ production}{Average\ solar\ intensity\ in\ 13\ hr.span} \ldots\ldots\ldots\ldots\ldots (13)$$

$$= \frac{2.43\ \times 10^3\ \times amount\ of\ distlled\ water\ (L)}{I_{avg.}\ \times\ 3600\ \times\ 13} \ldots\ldots\ldots\ldots (14)$$

6.7.2 Heating efficiency

Since PCM is used in this experiment, heating both PCM and water demands significant energy. Hence, heating efficiency needs to be analyzed to consider the heating of PCM and water as direct energy utilization. Although it is not affected by the solar still output, it considers only the heating of water and PCM (Lauric acid). So, it can be defined as the ratio of sensible and latent water heating and PCM to the average solar irradiance during working hours as Eq. (5). It can also be termed 'Direct efficiency.'

$$Heating\ efficiency\ (\eta_h) = \frac{Sensible\ and\ latent\ heating\ of\ water\ and\ PCM}{Average\ solar\ intensity\ in\ 13\ hr.span} \ldots (15)$$

$$= \frac{(mcdT)_w + (mcdT + mL)_{PCM}}{I_{avg.}\ \times\ 3600\ \times\ 13} \ldots\ldots\ldots\ldots\ldots\ldots\ldots\ldots (16)$$

Figure 6.36 shows the comparative study of all sets of analyses. That reflects the performance improvement of both solar stills with PCM and QD. QD improves the heat absorptance, and PCM can hold the heat for a time. Without PCM and QD, PSS yielded 1830 mL, 10.2% more than the CSS yield of 1660 mL. With PCM only, PSS yielded 2530 mL, 7.2% more than the CSS yield of 2360 mL. With QD and PCM, PSS yielded 3685 mL, 21.21% more than the CSS yield of 3040 mL. With QD, improvement was significant as compared to without QD.

With QD and PCM, yield improved by 100.1% in the case of PSS and 83.13% in the case of CSS compared to without QD and PCM.

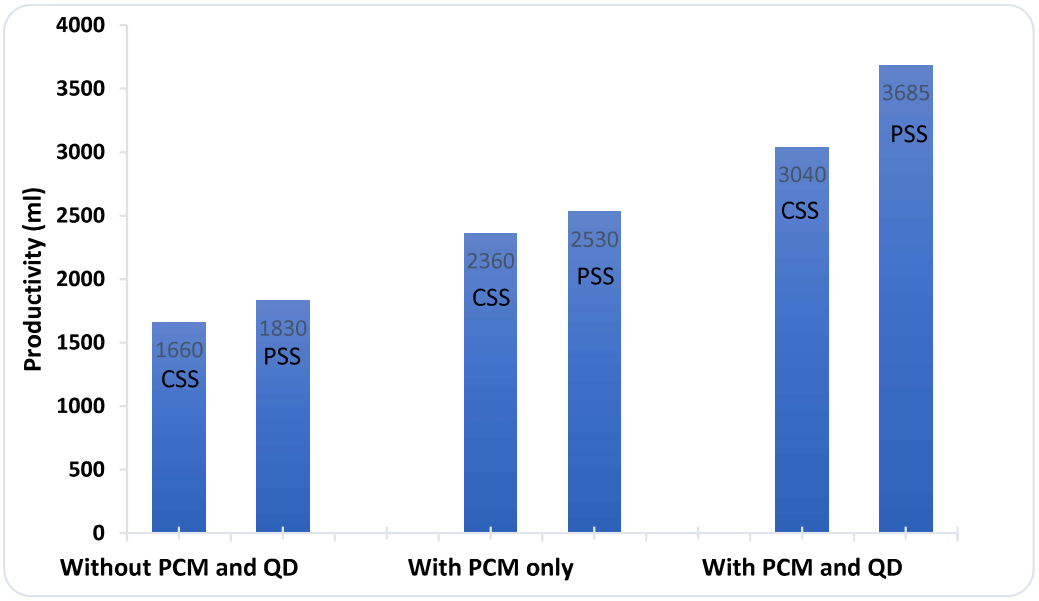

Figure 6. 36 Comparison of cumulative yield of all three set of arrangement of CSS and PSS.

The summary of outcomes of this experiment is listed in Table 6.3, which consists of total cumulative yield along with utilization and heating efficiencies for both CSS and PSS.

Table 6. 2 Summary of yield and efficiency of CSS and PSS

S.N.	Type of Arrangement	Solar Still	Cumulative Yield (mL/m^2)	Utilization efficiency	Heating Efficiency
1.	**Without PCM and QD**	*CSS*	1660	5.0%	19.72%
		PSS	1830	6.70%	25.59%
2.	**With PCM**	*CSS*	2360	16.75%	27.84%

		PSS	2530	15.98%	35.12%
3.	**With PCM and QD**	*CSS*	3040	21%	37.23%
		PSS	3685	27.53%	49.30%

6.7.3 Exergy analysis

Exergy efficiency can be defined as the ratio of the useful work output of the system to the reversible work output for energy-consuming systems. For solar still, it can be defined as the ratio of exergy output associated with the yield (distilled water) to exergy input (radiation energy) as expressed by Eq. (4).

The result shows that the exergy efficiency of PSS is better than the CSS type arrangement, and it further gets improved by adding PCM and QDs material. Figure 6.37 shows that the exergy efficiency reached 2.20% for PSS with PCM and QD compared to 1.79 % for CSS with a similar testing arrangement. Using QD material significantly improves the exergy efficiency of PSS and CSS by 117.8% and 105.74%, respectively, relative to PCM alone.

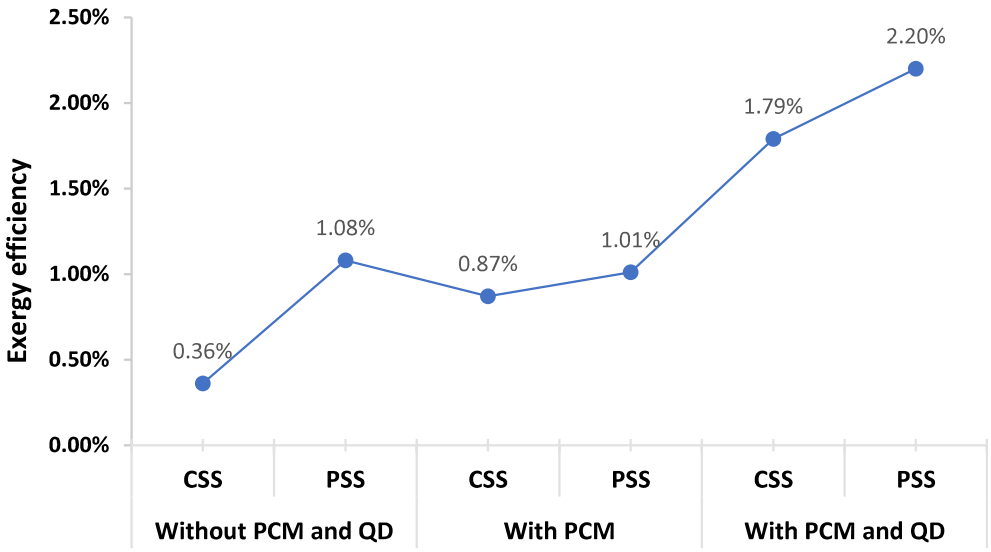

Figure 6. 37 Exergy comparison of solar stills

6.8 Distilled water quality

The palatability of water is measured in terms of taste, odor, colors, and turbidity at ambient temperature. The quality of distilled water obtained from solar still is compared from basin water, results are tabulated in table 6.3. Also compared with WHO standards of fresh water.

Table 6. 3 Water quality test results

S. No.	Parameters	Basin water	Distilled water	WHO standards
1.	Taste	Salty	Mild taste	***No taste***
2.	Color	Hazy transparent	Colorless	***Colorless***
3.	Odor	No odor	No odor	***Odorless***
4.	TDS (ppm)	730	75	***<600***

5.	pH	7.4	7.1	***6.5-8.5***
6.	Conductivity (mS/cm)	25	48×10^{-3}	***<250×10⁻³***

6.9 Uncertainty analysis

The approach of experimental uncertainty analysis examines a derived quantity based on the uncertainties in the experimentally measured quantities that are employed in some mathematical relationship ("model") to calculate that derived quantity. Based on that, the measured quantity is deemed to have internal uncertainty, and the uncertainty of the derived quantity is determined using the error propagation law. The following variables are measured during the experiment's total solar radiation, wind velocity, ambient temperature, glass cover temperature, saline water temperature, absorber plate temperature, PCM temperature, and the amount of fresh water. Table 3.6 shows the accuracy and range of the instruments and uncertainties of the measurements.

- **Internal Uncertainty**

The statistical analysis of the repeated measurement at each point put forward the "Internal Uncertainty", U_I. It should be noted that "N" measurements are taken, and then the average value for each measured quantity is determined. So, the best estimate of a quantity "X" for each operation point is the arithmetic mean $\bar{x}$ of the N observations of the quantity (x_j) and its internal uncertainty will be standard deviation (σ) of the mean, calculated by Eq. (17) as follow [130].

$$\sigma_{I,X} = \left(\frac{\sum_{j=1}^{N} \left(x_j - \bar{x}\right)^2}{N(N-1)} \right)^{0.5} \quad \ldots\ldots\ldots\ldots\ldots\ldots\ldots\ldots\ldots\ldots Eq.\,(17)$$

Internal uncertainties are inherently reliant on particular test conditions. As a result, it takes into account both fluctuations in the experimental settings not taken into account by the model as well as variations in the measured quantities during the experiment that are within the bounds set by the standards.

- **External Uncertainty**

The computation of uncertainties over the entire measurement, taking into account of all relevant data, such as measured and sensor uncertainty, etc., results in "External Uncertainty" or "Standard Uncertainty", U_E. The standards define the limits of the accuracy of the measurements. Accuracy (a) is a qualitative metric that indicates how close the result is to the true value of the measured quantity. The standard uncertainty for a given accuracy can be determined from a relation, provided the symmetric bound of accuracy has an equal likelihood of lying anywhere within bound, calculated by Eq. 18 as follow [130].

$$U_{E,x} = \left(\frac{a_x^2}{3}\right)^{0.5} \ldots\ldots\ldots\ldots\ldots\ldots\ldots\ldots\ldots\ldots\ldots\ldots Eq.(18)$$

If there are multiple independent sources of uncertainties, the resultant uncertainty is calculated by general law of uncertainty combination using Eq. (19).

$$U = \left(\sum_i U_i^2\right)^{0.5} \ldots\ldots\ldots\ldots\ldots\ldots\ldots\ldots\ldots\ldots\ldots\ldots Eq.(19)$$

Table 6. 4 Standard uncertainty of the measurements

Components	Accuracy	Range	Resolution	Standard Uncertainty
Solar power meter	±10 W/m^2	0-1999 W/m^2	1 W/m^2	4 W/m^2
K-class thermocouple	±1°C	-100^{0}C to 1300^{0}C	1°C	0.5 °C
Thermometer	±1 °C	-50 °C – 70 °C	0.5 °C	0.5 °C
Anemometer	±0.1 m/s	0.3-30 m/s	0.1 m/s	0.057 m/s

Measuring flask	±5 mL	0-1000 mL	10 mL	3 mL

- **Combined Uncertainty**

Generally, a variable 'Y' linearly depends on 'N' other independent variables X_1, X_2……..X_n like Y=f(X_1, X_2…..X_N). Then, the standard uncertainty in the estimate Y is obtained by the Law of error propagation. The reduced equation to estimate the uncertainty is

$$U_Y = \left(\sum_{i=1}^{N} \left(\frac{\partial f}{\partial x_i} \right)^2 U_{x_i}^2 \right)^{0.5} \ldots\ldots\ldots\ldots\ldots\ldots\ldots\ldots Eq.(20)$$

Like uncertainty involved in calculation of efficiency and yield can be calculated by above equation.

Uncertainty in Thermal Efficiency (η):

The efficiency is the function of solar flux and yield from Eq. 1. Hence, using Eq. 20.

$$U_\eta = \left[\left(\frac{\partial \eta}{\partial m} U_m \right)^2 + \left(\frac{\partial \eta}{\partial I} U_I \right)^2 \right]^{0.5}$$

$$U_\eta = 1.76$$

On average basis, 'm' was 0.113 kg and 'I' was 456 W/m^2. Uncertainty associated with m and I can be taken from Table 6.4. Similarly, uncertainty in exergy efficiency can be obtained.